TURUN
YLIOPISTO
UNIVERSITY
OF TURKU

ELECTROCATALYSTS FOR ENVIRONMENTAL MITIGATION

Synthesis, Characterization and Application

Adefunke O. Koyejo

TURUN YLIOPISTON JULKAISUJA – ANNALES UNIVERSITATIS TURKUENSIS
SARJA – SER. AI OSA – TOM. 711 | ASTRONOMICA – CHEMICA – PHYSICA – MATHEMATICA | TURKU 2024

TURUN
YLIOPISTO
UNIVERSITY
OF TURKU

ELECTROCATALYSTS FOR ENVIRONMENTAL MITIGATION

Synthesis, Characterization and Application

Adefunke O. Koyejo

TURUN YLIOPISTON JULKAISUJA – ANNALES UNIVERSITATIS TURKUENSIS
SARJA – SER. AI OSA – TOM. 711 | ASTRONOMICA – CHEMICA – PHYSICA – MATHEMATICA | TURKU 2024

University of Turku

Faculty of Science
Department of Chemistry
Chemistry
Doctoral programme in Exact Sciences
Materials Chemistry Research Group

Supervised by

Professor Carita Kvarnström
Department of Chemistry
University of Turku
Turku, Finland.

Adjunct Professor Pia Damlin
Department of Chemistry
University of Turku
Turku, Finland.

Reviewed by

Assoc. Professor Tanja Kallio
Department of Chemistry and
Materials Science
Aalto University
Espoo, Finland.

Professor Pawel Kulesza
Laboratory of Electroanalytical
Chemistry
University of Warsaw
Warsaw, Poland.

Opponent

Professor Csaba Janaky
Department of Physical Chemistry and
Materials Science
University of Szeged, Hungary

ISBN 978-951-29-9684-1 (PRINT)
ISBN 978-951-29-9685-8 (PDF)
ISSN 0082-7002 (Print)
ISSN 2343-3175 (Online)
Painosalama, Turku, Finland 2024

To family,
For all you are and
All you will continue to be.

UNIVERSITY OF TURKU
Faculty of Science
Department of Chemistry
Chemistry
ADEFUNKE O. KOYEJO: Electrocatalysts for Environmental Mitigation: Synthesis, Characterization and Application
Doctoral Dissertation, 122 pp.
Doctoral Programme in Exact Sciences (EXACTUS)
May 2024

ABSTRACT

The growing environmental crisis has strengthened interest in conversion technologies within the chemical industry, particularly in the reducing of greenhouse gases and minimizing toxic chemicals. To combat these issues, research and developmental technologies have focused on sustainable and environmentally friendly practices capable of reducing harm to humans and the environment. At the heart of these technologies is electrochemistry, which uses renewable energy sources and allows tuneable, selective, and scalable reactions. Electrochemical conversion provides a sustainable route to the production of essential fuels and commodity chemicals required globally. Due to its simplicity, electrochemistry can thus be applied to many synthetic reactions.

The primary goal of this research is to contribute to the ever-growing challenge observed in energy conversion and storage by synthesizing, characterizing, analysing, and evaluating electrocatalytic materials for carbon dioxide, CO_2 electrocatalysis and 4-nitrophenol, 4NP electrocatalysis. These two processes are pivotal in environmental remediation and eradication of toxic chemicals. Thus, developing a path free of fossil fuel for the production of commodity chemicals is the core of this research. Electrocatalysts consisting of metal nanoparticles (Au, Pd, Cu), metal oxide (TiO_2), layered double hydroxide, LDH (NiFe, CuFe) and graphene oxide, GO were synthesized and extensively characterized. Their activity was explored and compared for electrocatalytic applications (CO_2 and 4NP). All electrocatalysts synthesized in this work showed significant catalytic performance: Au/rGO being the most active for CO_2 electrocatalysis in non-aqueous solvents and Pd/TiO_2 the most active for 4NP electrocatalysis. Ternary catalysts (Cu-TiO_2/rGO) also displayed improved catalytic activity for electrochemical reduction of carbon dioxide, $ERCO_2$ in aqueous media. The enhanced performance of catalyst materials was linked to the synergy between the pure metals (Au, Pd, and Cu) and the multifunctional support (TiO_2, rGO).

This research also demonstrates the qualitative development of electrochemical analytical techniques for the selective detection of CO_2 reduction product. A rotating ring-disc electrode, RRDE was used as a quick analytical tool for the detection of acetic acid, AA, a product formed during $ERCO_2$ on the ternary Cu-TiO_2/rGO catalyst. Traditional characterization techniques such as nuclear magnetic resonance,

NMR spectroscopy and high-performance liquid chromatography, HPLC were further employed to confirm the detection of acetic acid.

Finally, the outcome of this research demonstrate that electrochemical techniques are a promising method for detection and conversion of CO_2 (and other toxic chemicals) to value added products in both academic laboratories and industries. This serves as a solid foundation in improving conversion technologies.

KEYWORDS: Electrocatalysis, CO_2, 4NP, nanoparticles, hybrid materials, supported nanomaterials, titanium dioxide, graphene oxide, copper, gold

TURUN YLIOPISTO
Matemaattis-luonnontieteellinen tiedekunta
Kemian Laitos
Kemia
ADEFUNKE O. KOYEJO: Electrocatalysts for Environmental Mitigation: Synthesis, Characterization and Application
Väitöskirja, 122 s.
Eksaktien tieteiden tohtoriohjelma (EXACTUS)
Toukokuu 2024

TIIVISTELMÄ

Ympäristöongelmien kasvaessa on kemianteollisuudessa herännyt lisääntynyt kiinnostus konversioteknologioita kohtaan, erityisesti kasvihuonekaasujen vähentämisessä ja myrkyllisten kemikaalien minimoimisessa. Näiden ongelmien ratkaisemiseksi tutkimus- ja kehitysteknologiat ovat keskittyneet kestäviin ja ympäristöystävällisiin käytäntöihin, jotka voivat vähentää haittoja ihmisille ja ympäristölle. Näiden teknologioiden keskiössä on sähkökemia, joka voi hyödyntää uusiutuvia energialähteitä ja mahdollistaa säädeltävät, selektiiviset ja skaalautuvat kemialliset reaktiot. Sähkökemiallinen konversio tarjoaa kestävän tavan välttämättömien polttoaineiden ja yleishyödyllisten kemikaalien tuotantoon maailmanlaajuisesti. Sähkökemiaa voidaan, sen yksinkertaisuuden vuoksi, soveltaa moniin eri synteesireaktioihin.

Tämän tutkimuksen päätavoitteena on vastata konversion ja varastoinnin kasvavaan haasteeseen. Tavoitteen saavuttamiseksi tutkimuksessa keskitytään hiilidioksidin (CO_2) ja 4-nitrofenolin (4NP) sähkökatalyysiin soveltuvien materiaalien syntetisointiin, karakterisointiin, analysointiin ja arviointiin. Nämä prosessit ovat avainasemassa ympäristön puhdistamisessa ja haitallisten kemikaalien neutraloimisessa. Tämän tutkimuksen keskeinen teema on fossiilivapaiden menetelmien kehittäminen hyödyllisten kemikaalien tuotantoon. Sähkökatalyytit, jotka koostuvat metallinanopartikkeleista (Au, Pd, Cu), metallioksideista (TiO_2), kerrostetuista kaksinkertaisista hydroksideista, LDH (NiFe, CuFe) ja grafeenioksidista (GO), syntetisoitiin ja karakterisoitiin monipuolisesti. Niiden aktiivisuutta tutkittiin ja verrattiin sähkökatalyyttisissä sovelluksissa (CO_2 ja 4NP). Kaikki tässä työssä syntetisoidut sähkökatalyytit osoittivat merkittävää katalyyttistä suorituskykyä: Au/rGO oli aktiivisin CO_2-sähkökatalyysissä orgaanisissa liuottimissa ja Pd/TiO_2 aktiivisin 4NP-elektrokatalyysissä. Ternaariset katalyytit (Cu-TiO_2/rGO) osoittivat myös selkeää katalyyttistä aktiivisuutta hiilidioksidin sähkökemiallisessa pelkistyksessä ($ERCO_2$) vesiliuoksessa. Katalyyttimateriaalien parantunut suorituskyky liittyi puhtaiden metallien (Au, Pd ja Cu) ja tukimateriaalien (TiO_2, rGO) väliseen synergiaan.

Tutkimus osoittaa myös sähkökemiallisten analyyttisten tekniikoiden laadullista kehittämistä CO_2-pelkistystuotteiden selektiiviseen havaitsemiseen. Pyörivää rengas-levyelektrodia (RRDE) käytettiin nopeana analyyttisenä työkaluna etikkahapon (AA) havaitsemiseen, jota muodostuu $ERCO_2$:n aikana ternaarisella Cu-TiO_2/rGO-

katalyytillä. Perinteisiä karakterisointitekniikoita, kuten ydinresonanssispektroskopiaa (NMR) ja korkean suorituskyvyn nestekromatografiaa (HPLC), käytettiin lisäksi etikkahapon tunnistamiseen.

Tämän tutkimuksen tulokset osoittavat, että sähkökemialliset tekniikat ovat lupaavia hiilidioksidin (ja joidenkin myrkyllisten kemikaalien) havaitsemiseen ja muuntamiseen hyödyllisemmiksi tuotteiksi sekä akateemisissa laboratorioissa että teollisuudessa. Sähkökemialliset prosessit ovat merkittävässä osassa konversioteknologioiden parantamisessa.

ASIASANAT: sähkökatalyysiin, hiilidioksidin, 4-nitrofenolin, ternaariset katalyytit, metallinanopartikkeleista, tukimateriaalien, grafeenioksidista, hiilidioksidin

Table of Contents

Abbreviations

[Emim][NTf_2]	1-ethyl-3- methylimidazolium bis(trifluoromethylsulfonyl)imide
[Hmim][BF_4]	1-hexyl-3- methylimidazolium tetrafluoroborate
4NP	4-nitrophenol
AA	Acetic acid
ACN	Acetonitrile
CA	Chronoamperometry
CE	Counter electrode
CCD	Charged coupled device
CTAB	Cetrimethyl ammonium bromide.
CV	Cyclic voltammetry
DMF	Dimethylformamide
DTGS	Deuterated triglycine sulphate
$ERCO_2$	Electrochemical reduction of CO_2
FA	Formic acid
FTIR	Fourier transform infrared spectroscopy
GCE	Glassy carbon electrode
GO	Graphene oxide
HPLC	High performance liquid chromatography
KCl	Potassium chloride
LDH	Layered doubled hydroxide
LSV	Linear sweep voltammetry
MOF	Metal organic framework
NMP	N-methyl-2-pyrrolidone
NMR	Nuclear magnetic resonance
NPs	Nanoparticles
PTFE	Polytetrafluoroethylene
PVA	Polyvinyl alcohol
PVP	Polyvinylpyrrolidone
RE	Reference electrode
rGO	Reduced graphene oxide
RDE	Rotating disc electrode

RHE	Reversible hydrogen electrode
RRDE	Rotating ring disc electrode
RRE	Rotating ring electrode
RT	Room temperature
RTILs	Room temperature ionic liquids
SCE	Saturated calomel electrode
SEM	Scanning electron microscopy
$TBAPF_6$	Tetrabutylammonium hexafluoroborate
TEM	Transmission electron microscopy
TGA	Thermogravimetric analysis
TiO_2	Titanium dioxide
UV-Vis	Ultraviolet visible spectroscopy
WE	Working electrode
XPS	X-ray photoelectron spectroscopy
XRD	X-ray diffraction

Symbols

µl	Microlitre
Ag	Silver
Ag/AgCl	Silver/Silver chloride
Au	Gold
Cu	Copper
Fc	Ferrocene
Fe	Iron
mg	Milligram
N_2	Nitrogen
Ni	Nickel
nm	Nanometre
Pd	Palladium
Pt	Platinum

List of Original Publications

This dissertation is based on the following original publications, which are referred to in the text by their Roman numerals:

I **Adefunke O. Koyejo**, Lokesh Kesavan, Pia Damlin, Mikko Salomäki, Jenevieve G. Yao, Minna Hakkarainen, Carita Kvarnström. Cellulose-Based Reduced Nanographene Oxide on Gold Nanoparticle Supports for CO_2 Electrocatalysis. *ChemElectroChem*, 2020; 7, (24), 4889–4899

II **Adefunke O. Koyejo**, Lokesh Kesavan, Pia Damlin, Mikko Salomäki, Carita Kvarnström. Synthesis of Layered Double Hydroxides and TiO_2 supported metal nanoparticles for electrocatalysis. *ChemElectroChem*, 2022; 9, (12), e202200442

III **Adefunke O. Koyejo**, Xia Chu, Lokesh Kesavan, Pia Damlin, Carita Kvarnström. Electroreduction of CO_2 by Hybrid Cu-TiO_2/rGO: Qualitative Detection using Rotating Ring Disc Electrode. *Manuscript submitted to ChemElectroChem*.

Contribution of the author:

Paper I, II & III: The author designed the study together with the supervisors, fabricated, synthesized, characterized the materials, collected, interpreted, and analysed data. The author wrote the first draft of the manuscript and contributed to its several revisions.

1 Introduction

1.1 Electrocatalysis: an overview

Electrocatalysis is a branch of chemistry that bridges electrochemistry and catalysis. It is often thought of as an extension of catalysis. A generally accepted definition of catalysis is a process that increases the rate of a chemical reaction through the addition of substances (catalyst) that do not themselves show a permanent chemical change. Catalysis can be classified into two types based on the phase of the catalyst relative to the reactant: homogeneous catalysis, where the catalyst is in the same phase as the reactant, and heterogeneous catalysis, where the catalyst is in a different phase than the reactant. Therefore, electrocatalysis is a form of heterogeneous catalysis that increases the rate of an electrochemical reaction, while catalysis is concerned with speeding up the rate of a chemical reaction [1]. The main feature of heterogeneous electrocatalysis is the transfer of electrons between the electrode and the reactant. Electrocatalysis is of great importance today, as it is essential for clean conversion technologies, energy storage, and electrosynthesis techniques used in electrochemical conversion processes. Electrocatalysis is particularly useful as it uses renewable energy sources and replaces the need for harsh reactions and corrosive reagents. Hence, electrocatalysis is the key to a sustainable future.

In practice, electrocatalysis is a clean and renewable energy technology [2] that plays a significant role in the actualization of a sustainable future [3]. Electrocatalysis is the key to the 2030 sustainable development agenda adopted by the United Nations (UN) member states. Electrocatalysis advances several of the UN sustainable development goals (SDGs) by offering solutions that address global challenges relating to clean energy (SDG 7), climate action (SDG 13), clean water (SDG 6), innovation (SDG 9), economic growth (SDG 8), sustainable cities and communities (SDG 11), life on land (SDG 15) and partnerships for goals (SDG 17). Electrocatalysis can be used to create a fossil fuel-free economy by either closing the carbon cycle and reducing CO_2 to value-added chemicals or creating an energy system based on hydrogen production through solar-driven water electrolysis. It can also be used for the removal or conversion of toxic chemicals from waste to other useful products [4].

Therefore, the importance and benefits of electrocatalysis in sustainability are evident, but not without limitations. A major challenge that exists is the development of low-cost stable, selective, and highly active electrocatalysts. Catalyst stability and durability are critical factors for electrocatalytic applications, as many catalysts suffer from degradation over time. Furthermore, catalyst poisoning by impurities or intermediates can significantly hinder the catalyst's performance. Some literature reports have focused on the design and optimization of electrocatalysts to improve performance, stability, and resist poisoning. These electrocatalysts consist of chemical catalysts (such as: metals and their alloys or metal oxides), biocatalysts (such as enzymes and other bio-based compounds) or pure metal electrodes.

1.2 Factors influencing electrocatalysis

Several factors affect electrocatalysis and altogether impact the overall performance of an electrochemical system. Variables that interact to determine the rate of an electrocatalytic reaction include the electrode material, the nature and composition of electrocatalytic materials and support (size and shape of materials, surface structure, morphology, and catalyst-support interaction), type of solvent, the reactant composition, temperature, interface properties, porosity, charge transfer, applied potential, catalyst active sites, and mass transport.

1.2.1 Electrode material

Different types of electrodes have been explored by literature with the aim to achieve high performance and increase the rate of catalytic reactions. Other than the standard solid electrodes such as glassy carbon, platinum, and gold, there are others made of metal nanoparticle or composite material, which are deposited on the electrode surface. The glassy carbon electrode, GCE is highly advantageous for electrocatalytic applications due to its affordability and exceptional electrical conductivity. GCE is also the most suitable electrode for doping or drop casting catalyst materials due to its chemical stability, electrochemical inertness across a wide potential range, and the ease at which it can be modified. The choice of electrode material is particularly important because the electrodes conduct electrons in the reaction and are invariably responsible for the yield and selectivity. When a catalyst material is deposited on the electrode, it is noteworthy that both catalyst and electrode can contribute to the electrochemical reaction. Thus, when using a catalyst modified electrode, it is important to choose an electrode that is inactive to the particular electrocatalytic reaction. In this research, the GCE was chosen due to its inactivity/limited activity in the electrocatalytic reactions of choice. This was done to ensure there were no side reactions erupting as a function of the bare electrode

material. For all electrochemical reactions studied in this research, the synthesized catalysts were drop-casted on GCE to produce a catalyst modified GCE.

1.2.2 Catalyst composition

Catalyst composition plays a significant role in electrochemical activity and selectivity. Several catalyst materials have been investigated concerning electrochemical reactions, but the choice of catalysts and catalyst composition is dependent on the desired objectives. For example, noble metals such as platinum (Pt) and palladium (Pd) are mainly used for fuel cell application. Gold (Au) is a model catalyst used in conversion technologies, e.g. for the conversion of CO_2 to CO, copper (Cu) is used for the conversion of CO_2 to multicarbon compounds and layered double hydroxides, LDH are used for oxygen evolution reactions, OER [5]. Aside from the enhanced electrocatalytic capabilities that the bulk metals possess, other parameters such as particle size, shape, and chemical composition can be functionalized to provide an electrode/electrolyte interface that further enhances electrocatalysis. This is done by leveraging the effect of area, crystal plane, and synergistic effect between components [6]. Hebie *et al.,* among several other literature reports, studied the shape and size dependent electrocatalytic activity of gold nanoparticles and reported the improvement in catalytic activity of smaller sized nanoparticles compared to the shape dependent nanoparticles. The improved activity of shape dependent nanoparticles was attributed to their structure and coordination number [7–9]. This research explores several catalyst compositions comprising of metal, non-metal, metal oxides and LDH for electrocatalytic reactions.

1.2.3 Solvent or electrolyte

The solvent or electrolyte typically functions as the medium where electrolyte salts (supporting electrolytes) are dissolved. These electrolytes can range from organic, and inorganic to aqueous solutions, forming a homogeneous solvent. Once the supporting electrolyte salts dissolve, they undergo ionization to form charged ions. During electrocatalysis, these charged ions are set in motion and a conductive path is created with the external circuit electrons. While electrons are transferred from the electrode to the adsorbed reactants via the external circuit, ions within the electrolyte solution migrate to counterbalance the charge, thereby closing the electrical circuit [10]. However, the electrolyte could decompose at the electrode surface, which negatively affects the stability of the electrochemical reaction. Therefore, it is important to determine the potential window for electrochemical stability of the electrolyte before conducting an experiment. This ensures that the electrolyte does not decompose in the potential range under study. Thus, the choice of solvent or

electrolyte solution in an electrocatalytic reaction determines the surface properties, kinetics and mechanism of the reaction through its interaction with the reactant, intermediate and product. In this research, room temperature ionic liquids, RTILs, organic (acetonitrile, ACN) and aqueous solutions were used with two supporting electrolyte salts: $KHCO_3$ and $TBAPF_6$.

1.2.4 Catalyst support

Nanoparticles such as Cu are suitable for electrochemical reactions; however, their fast deactivation limits them. The use of support materials provides stability and easier dispersion of nanoparticle catalysts. As mentioned above, catalytic activity of nanoparticles depends on the particle size and dispersion, but the support affects the particle size and degree of dispersion. Thus, the properties of the support material play a significant role in enhancing electrocatalysis. Some common support materials consist mainly of carbon, such as carbon nanotubes (CNT) and graphene. With their strong electrical conductivity and chemical stability, these materials provide support for the nanoparticle by improving adhesion and promoting the formation of smaller sized nanoparticles. In addition to carbon, other support materials such as metal oxides (TiO_2) have been employed for their enhanced chemical stability and ability to form a strong bond with metal nanoparticles [11]. Two types of catalyst support were employed in this research: the semiconducting TiO_2 and reduced graphene oxide, rGO both advantageous in the distribution of metal nanoparticles.

1.2.4.1 Graphene-type materials as a catalyst support

There has been a growing attraction in recent times for graphene and graphene-like materials (graphene, reduced graphene oxide, rGO, carbon nanotube, CNT, carbon nanofiber, CNF, etc.) as substrates for electrocatalysts. Graphene, an allotrope of carbon, is a two-dimensional (2D) material with unique characteristics and enhanced surface area. Although, the category of 2D nanomaterials has experienced rapid growth, expanding beyond graphene to include LDH, carbon nitrides, MXenes, and other metal-organic frameworks, MOFs. 2D materials are special and easily modified which makes them pivotal in driving advancements in material innovation and enhancing material properties [12]. Therefore, it is no surprise that graphene, a 2D material, is regarded as the wonder material of the future [13].

Scientific enthusiasm for graphene materials stems from their superior electrical, mechanical, thermal, and optical properties. Graphene can be synthesized through various methods, such as the mechanical exfoliation of graphite, epitaxial growth, chemical vapour deposition, CVD, and the reduction of graphene oxide, GO.

Although, other methods produce perfectly structured graphene, the reduction of graphene oxide is still the most viable route because it offers a cost-effective method to produce a graphene-like structure [14].

The investigations on the synthesis of GO began more than 150 years ago [15]. Since then, there has been an increased variety of graphene-based materials available commercially and in laboratories through synthesis. Earlier literature has focused on synthesis methods developed by Brodie [16], Staudenmaier [17], Hummers [18], and the Tour method [19]. However, the modified Hummers method is still the most popular technique for GO synthesis from inexpensive graphite due to its simplicity and high yield. In the modified Hummers method, graphite is oxidized by strong oxidants, to form a stable GO solution. This GO solution can subsequently undergo reduction using various reduction methods to replicate the graphene-like structure.

While the modified Hummers method is a reliable and well-established method for graphene production, the concern and interest in environmental sustainability has motivated research into investigating the potential of generating graphene from renewable sources. The use of biomass as a source of carbon presents a greener alternative for graphene production. This renewable material has been explored in industrial applications in the form of biofuel, biogas, and bioenergy. In graphene production, the biomass undergoes several pre-treatment methods to break down the intricate structure, remove volatile compounds and increase the carbon content of biomass [20–23]. Due to the variety of methods in which graphene-like materials can be produced, their properties and performance vary depending on the precursor material and reduction process.

In this research, graphene-based materials were synthesized, characterized, and used as nanoparticle support (paper I and III). In paper I, we introduced a new and novel graphene-like catalyst support based on cellulose (nGO) [24,25]. The graphene structure was restored by exploring two reduction methods (i) caffeic acid and (ii) water at a temperature of 180 °C. This method is environmentally sustainable as opposed to others requiring strong reductants. The physicochemical properties of the cellulose derived graphene material were studied and its performance as a suitable catalyst support was evaluated. Paper III focused on the use of GO produced from the modified Hummers method as nanoparticle support. The performance of these materials on electrocatalytic reactions was investigated.

1.2.4.2 Titania – based material as a catalyst support

The importance of catalyst support has been discussed earlier. Asides from graphene, a commonly used metal oxide catalyst support material is titanium dioxide (TiO_2). TiO_2 is the material of choice due to its tunability, high thermal stability and mechanical strength. It is also affordable, nontoxic and possesses a

high corrosion resistance. Its electronic and optical properties make it a material of interest in many photochemical and electrochemical applications. TiO_2 exists in three crystalline phases: anatase, rutile and brookite, with the anatase being the most thermally stable [26] and the rutile being the most thermodynamically stable. The anatase and rutile phases are tetragonal in structure while the brookite has an orthorhombic structure. The phase composition of the titania support determines the overall activity of the catalyst. A strong metal-support interaction is observed in anatase titania while the rutile and brookite phases are known to have weaker metal-support interaction [27].

Numerous studies have investigated the multifaceted applications of titania, examining its role as a catalyst and a supporting material in its various forms, including nanoparticle (0D), nanorod (1D), and nanosheet (2D). Transition and non-transition metals have been anchored on TiO_2 and applied in photochemical and electrochemical reactions. The presence of a hypo-d-electron feature, which interacts with noble metals (especially Pt) and changes their catalytic activity by modifying their surface interaction energy, is observed. This takes place with a shift in the d-bond with respect to the Fermi level [28]. This characteristic makes TiO_2 a good support. Titania used in catalysis can either be synthesized from scratch or purchased commercially. Several methods have been reported for the synthesis of titania including, hydrothermal [29], electrochemical [30], and solgel methods [31]. It is important to note that synthesis conditions influence the physicochemical properties of titania, and these factors have a direct impact on the material's performance.

In this research, commercially available Degussa P25 TiO_2 was used as nanoparticle support. The Degussa titania consists of both anatase and rutile phases with the anatase existing predominantly. Au, Pd and Cu was anchored on TiO_2 (Paper II and III) and employed as electrocatalyst for 4NP and CO_2 electrocatalysis. In paper III, a binary composite of TiO_2 and GO was first synthesized, and Cu was immobilized on the TiO_2/rGO support.

1.3 Applications of electrocatalysis

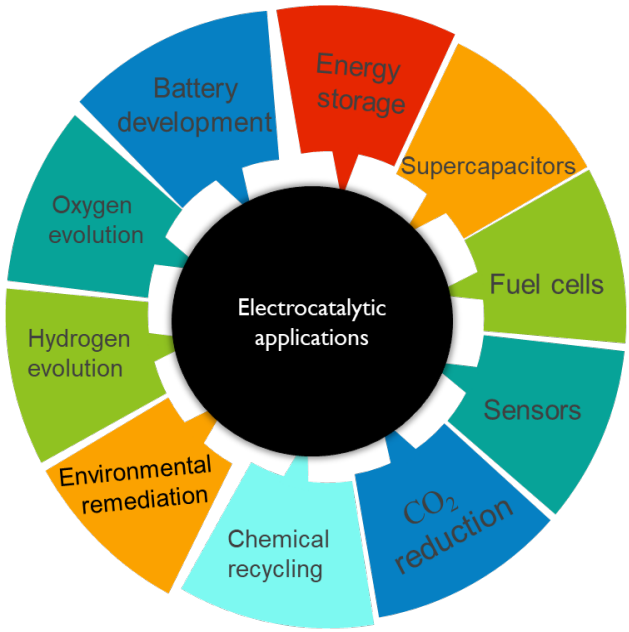

Figure 1. Schematic presentation of practical applications of electrocatalysis.

Nowadays, electrocatalysis is applied to several fields (Figure 1) due to its application as a clean and green energy technology. It is particularly significant in energy conversion and storage. Electrocatalysis can be used in fuel cells, electrolysers (electrochemical water splitting), oxygen evolution reaction (OER), hydrogen evolution reaction (HER) and CO_2 conversion technologies. In addition, electrocatalysis is useful in chemical synthesis and chemical recycling by aiding the conversion of reactants into desired products. Another significant application of electrocatalysis is environmental remediation, especially in wastewater treatment. Electrocatalysis has been employed to remove pollutants such as 4NP from wastewater streams by enhancing the oxidation and reduction of organic or inorganic compounds leading to their conversion, degradation, or complete removal.

1.4 Objectives of the research

Electrocatalysis offers a future centric approach to the production of value-added chemicals. Yet, stable, and effective catalysts are required to drive specific reactions. Therefore, this research focuses on contributing to sustainability by synthesizing and screening materials for different electrocatalytic applications. At the core of these electrocatalytic applications are CO_2 electrocatalysis and 4NP electrocatalysis, which are relevant to environmental remediation.

The main objectives of this research are:

- To discover, synthesize and optimize suitable materials (supported metal nanoparticles and LDH) for electrocatalysis.
- To thoroughly characterize the structure, composition and properties of synthesized catalysts using state-of-the-art techniques such as FTIR, XRD, XPS, Raman, TEM etc.
- To demonstrate the suitability of materials in electrochemical applications.
- To evaluate the performance of nanoparticles with different transition metal centres for 4NP electrocatalysis.
- To introduce and explore the RRDE as a novel analytical tool for detecting products formed during $ERCO_2$.

2 Electrocatalytic Reactions

2.1 CO_2 electrocatalysis

Carbon dioxide (CO_2) plays a prominent role in providing the carbon source required to support life on earth. For centuries, CO_2 emissions have been regulated by plants and other natural organisms through a process called photosynthesis. This photosynthetic activity helps maintain a closed carbon cycle by balancing CO_2 consumption and CO_2 emission. However, current industrial processes originating from the combustion of hydrocarbons and fossil fuels have produced more CO_2 than nature can control, resulting in a high concentration of CO_2 in the atmosphere. Today, CO_2 makes up for approximately 80 % of the greenhouse gases (GHG), a chief culprit in climate change. The growing environmental challenges have prompted new regulations and stimulated interest in CO_2 electrocatalysis. The electrochemical conversion of CO_2 ($ERCO_2$) focuses on converting CO_2 into other valuable chemicals and offers a renewable alternative to fossil fuels. Electrocatalysis offers a suitable route to overcome the barrier of transformation encountered during

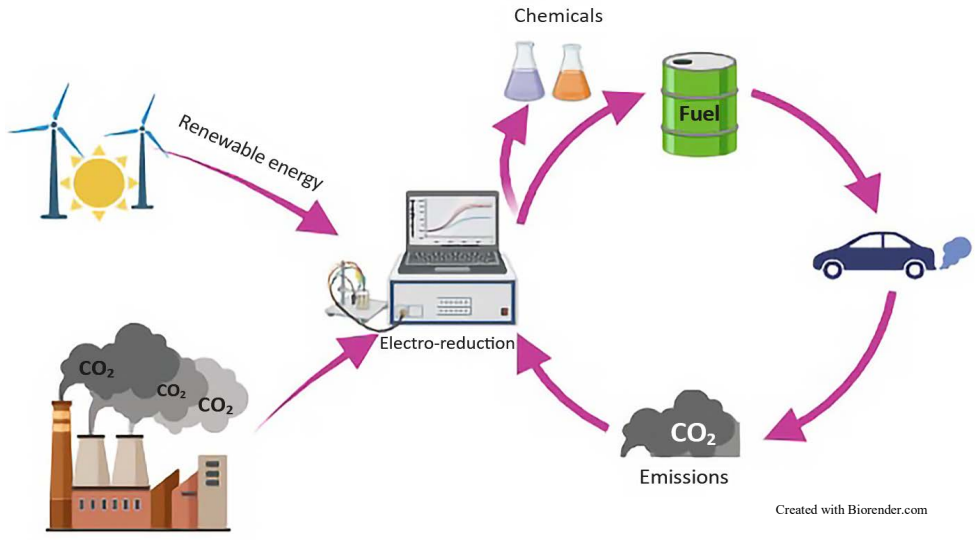

Figure 2. Illustration of the carbon cycle.

the reduction of the thermodynamically stable CO_2 molecule. This phenomenon is a key element in closing the anthropogenic carbon cycle (Figure 2) and reducing CO_2 emissions-related energy and environmental problems. However, still characterized by its high overpotential and poor selectivity, the reduction of CO_2 to value added chemicals poses a challenge. To combat these problems, research is focused on optimising electrocatalyst and electrolyte systems [32,33].

2.1.1 Non-aqueous electrolytes for CO_2 electrocatalysis

The choice of electrolyte used in CO_2 reduction plays a vital role in product formation. Typically, aqueous electrolytes are most suitable for CO_2 electrocatalysis because of their wide range of product formation, but non-aqueous solvents have several advantages over the aqueous solvents, such as: the solubility of CO_2 in aqueous electrolytes, which is approx. 34 mM under standard conditions, compared to a 270 mM CO_2 solubility in ACN. Low CO_2 solubility limits the mass transfer in the electrochemical system. Another advantage of the non-aqueous electrolyte is the wide potential window and lower proton concentration, which inhibits the unwanted production of hydrogen, thus avoiding hydrogen evolution reaction (HER). $ERCO_2$ in non-aqueous solvents forms the basis of CO_2 sensors. Literature on $ERCO_2$ in non-aqueous electrolyte has reported the formation of CO, CO_3^{2-} and oxalate. Formation of the CO intermediate is a key step in CO_2 electrocatalysis, as proposed by mechanisms found in the literature. Kumar *et al.* reported that $ERCO_2$ in dimethylformamide, DMF and n-methyl-2-pyrrolidone, NMP yield mostly oxalate [34]. From the work of Welford *et al.* [35] for $ERCO_2$ in aprotic media, a mechanism is proposed (equation (1) and (2)) for the formation of oxalate and CO.

$$2CO_2 + 2e^- \rightarrow C_2O_4^{2-} \quad (1)$$

$$2CO_2 + 2e^- \rightarrow CO + CO_3^{2-} \quad (2)$$

Although, the solubility of CO_2 in organic solvents is relatively high, the lack of a proton source limits its product formation. Alternatively, organic/aqueous solvent mixtures can be used to enhance solubility (in aqueous media) and provide an additional proton source (in non-aqueous media). Literature reports a different product pathway in H_2O containing non-aqueous electrolytes. For example, $ERCO_2$ in ACN produced CO, while $ERCO_2$ in ACN/H_2O mixture produced formate [36], [37]. Therefore, encouraged by the solubility of CO_2 in ACN, coupled with its ability to produce a known product (CO) during $ERCO_2$ and its miscibility with 4NP, this research explores the use of ACN as an electrolyte for CO_2 (paper I) and 4NP electrocatalysis (paper II).

2.1.1.1 RTIL as an electrolyte for CO_2 electrocatalysis

Another non-aqueous electrolyte that is currently emerging for CO_2 electrocatalysis is the room temperature ionic liquids, RTILs. RTILs are liquid based organic salts consisting of an asymmetric cation and a small size inorganic anion that offer electrolyte stability and a wide potential window for electrocatalytic applications [38]. They can be used as bare electrolytes or be added to water or other organic solvent to create an electrolyte mixture. The significant advantages of RTILs are their tunability, low viscosity and volatility, high chemical and thermal stability and high CO_2 solubility. Thus, they serve as a green alternative to organic solvents. By modifying the cations and anions, one can obtain a RTIL with the desired properties. The cationic and anionic effect of RTIL has been investigated for ERCO_2. Anions such as trifluoroacetate, triflate, acetate, triazolide, tetrafluoroborate, and so on have been reported and their effect extensively studied [39,40]. The research proposes that CO_2 reduction to CO is through a cation effect. In this process, the imidazolium cation binds to CO_2 radical ion and forms a [Emim]-CO_2 (1-ethyl-3-methylimidazolium- CO_2) complex at the electrode surface, which stabilizes reaction intermediates, lowers energy barriers and improves CO_2 reduction [41]. Studies in RTIL/H_2O electrolyte mixtures have reported the reduction of CO_2 at less negative potential than pure RTILs [42]. Other electrolyte mixtures including RTILs/ACN, and ternary electrolyte mixtures (RTIL/ACN/H_2O) have also been explored in the literature [43]. Based on this, RTIL with imidazolium-based cation ([Hmim][BF_4]) and [Emim][NTf_2]) was investigated as electrolytes for CO_2 electrocatalysis (paper I).

2.1.2 Aqueous electrolyte for CO_2 electrocatalysis

Aqueous electrolytes are most attractive and popular for CO_2 electrocatalysis as they provide the necessary proton source to convert CO_2 to hydrocarbons. However, in contrast to other electrochemical reactions involving O_2 and H_2, CO_2 electrocatalysis involves several reaction intermediates and pathways, which gives rise to a variety of products including CO, formate, methane, methanol, ethylene, oxalic acid, formic acid, acetic acid and more (Table 1). To achieve these product formations, multiple transfers of protons and electrons are required. A major challenge of the aqueous electrolyte system is the competing hydrogen evolution reaction (HER), which may occur at the same potential range where CO_2 electrocatalysis takes place [44]. Another challenge is the difficulty associated with CO_2 activation and the need to overcome a large energy barrier to form intermediates. Table 1 shows the different products detected and reported during CO_2 reduction and their equilibrium potentials. It is noteworthy that depending on the composition of the electrocatalytic system (catalyst, solvent, electrolyte, pH etc.), different product is possible. As observed,

$ERCO_2$ by one electron demands substantial energy and results in the formation of CO_2 radical anion ($CO_2^{-\cdot}$), which poses a challenge for generating valuable organic compounds. Consequently, achieving multi-electron reductions is necessary for a green and sustainable CO_2 conversion [45].

Table 1. CO_2 half reactions [46–48].

Half reaction (at pH 7)		E^O (V *vs.* SHE)
$CO_2 + e^- \rightarrow CO_2^{-\cdot}$		-1.90
$CO_2 + 2H^+ + 2e^- \rightarrow HCOOH$	Formate	-0.61
$CO_2 + 2H^+ + 2e^- \rightarrow CO + H_2O$	Carbon monoxide	-0.52
$CO_2 + 2e^- \rightarrow C_2O_4^{2-}$	Oxalate	-0.59
$CO_2 + 4H^+ + 4e^- \rightarrow HCHO + H_2O$	Formaldehyde	-0.48
$CO_2 + 6H^+ + 6e^- \rightarrow CH_3OH + H_2O$	Methanol	-0.38
$CO_2 + 8H^+ + 8e^- \rightarrow CH_4 + 2H_2O$	Methane	-0.24
$2CO_2 + 7H^+ + 8e^- \rightarrow CH_3COO + 2H_2O$	Acetate	-0.29
$2CO_2 + 12H^+ + 12e^- \rightarrow C_2H_5OH + 3H_2O$	Ethanol	-0.33
$2CO_2 + 12H^+ + 12e^- \rightarrow CH_2CH_2 + 4H_2O$	Ethylene	-0.35
$2H^+ + 2e^- \rightarrow H_2$		-0.41

2.1.3 Catalysts for CO_2 electroreduction

CO_2 being a chief culprit in greenhouse gases has gained global attention. Efforts have been made to convert it to other value- added chemicals. $ERCO_2$ is a sustainable method to utilize CO_2 as a bulk chemical and close the carbon cycle (Figure 2). However, the bottleneck is the availability and development of catalysts that provide reactive sites for $ERCO_2$ and enhance its scalability. There have been several reported heterogeneous catalysts for CO_2 electrocatalysis. Many are based on pure metals such as Au, Pd and Cu, others involve the use of alloys and recently, composites consisting of metals and/or non-metals have also been explored.

Pure metals: $ERCO_2$ on pure metals (noble and transition) dates back to the 1950s, when Hori *et al.,* experimented on polycrystalline metal electrodes. This birthed other studies on the use of metal electrodes (Pb, Hg, Ti, Au, Ag, Zn, Cu etc.), which are selective to the production of CO. Of all the studied metals, Cu showed a unique ability to produce hydrocarbons, aldehydes and alcohols [49]. Other transition metals reported by literature include Sn, In, and Pb, which are selective to the formation of $HCOO^-$ [50]. Thus, Cu is considered the benchmark metal catalyst for CO_2 reduction

due to its high activity and selectivity towards multicabon, C_{2+} products. Considerable efforts have since been focused on exploring Cu in the pure metallic form and as a composite for $ERCO_2$.

Alloys: Some researchers have reported advancements in enhancing the efficiency of $ERCO_2$ through the utilization of alloys. Improvement in the electrochemical properties such as onset potential, and current response have been reported. Alloying has been reported to show improved electrocatalytic activity towards $ERCO_2$ than their pure metal counterparts. Some examples of binary and tertiary alloys reported in the literature for $ERCO_2$ are AuPd, AuCu, CuBi, CuZn, Pb-Bi-Sn [51–54] etc, many of which are selective to the formation of formate.

Non-metals: Doped and undoped carbon materials such as graphene, carbon nanotubes/nanofibers and diamonds have been investigated as catalyst for $ERCO_2$. Some dopants used include nitrogen, boron, etc. Although these materials may be environmentally friendly, and metal-free, their use is limited to the production of CO [55–57].

Metal/non-metal composites: Various metal/non-metal composites and metal supported composites have also been explored for $ERCO_2$. Some of these composites can be a mixture of metal, metal oxide and non-metal to form ternary composites or supported metal catalysts [58–60]. All of which offer higher activity to $ERCO_2$ than pure metals alone. Other types of catalyst materials currently explored in literature for $ERCO_2$ are molecular catalysts [61–66], MXenes [67–70] and LDH [71–74].

2.2 4NP electrocatalysis

4-nitrophenol, 4NP is an organic compound involved in a number of manufacturing processes, including pigment, pharmaceuticals and agricultural products. Its wide industrial application makes 4NP a toxic compound with adverse effects on humans, plants, and the environment [75]. Even low concentrations are detrimental to human health and may possess mutagenic and carcinogenic properties. 4NP can penetrate the bloodstream either through contact with the skin or by inhalation. Once inside the bloodstream, it undergoes biotransformation into harmful substances, leading to various adverse effects. Inhaling or ingesting 4NP in large amounts can result in symptoms like headaches, drowsiness, nausea, and the development of cyanosis in the lips, ears, and fingernails. Furthermore, when 4NP comes in contact with the eyes, it can lead to irritation [76]. With its continuous use and release to the atmosphere, rivers, and seas, 4NP has earned its way to the list of top priority pollutants in many countries. Several efforts have since then been utilized for the

detection, reduction, and elimination of 4NP such as: chemical reduction, biodegradation, chromatography, and electrochemical methods [75]. By taking advantage of low-cost electrochemical techniques, as opposed to other methods (chemical reduction) that require huge running costs, the use of toxic reducing agents is eliminated. 4NP is generally converted to hydroxylaminophenol, 4AP, which is a less toxic precursor compound that serves as an intermediate in the production of dyes, agrochemicals, and compounding of drugs such as paracetamol and acetaminophen [77]. The electrocatalytic conversion of 4NP offers a straightforward, easy to control, higher efficiency and environmentally friendly reaction [78]. The ease of the electroreduction of 4NP has made it a model compound for the testing of catalyst materials.

Several mechanisms have been proposed for the heterogeneous reduction of 4NP in aqueous and non-aqueous solvents. In aqueous solvent, a pH dependent mechanism reported involves a direct four-electron and four-proton transfer process, which reduces the 4NP to 4AP. During the electrochemical process, an additional reversible peak is observed which is attributed to the two-electron, two-proton transfer from hydroxylaminophenol to nitrosophenol [79]. In non-aqueous solvent, a self-protonation reaction proceeds the formation of the 4-nitrophenolate ion, which undergoes further reaction to produce 4AP. Altogether, the formation of 4AP from 4NP in an aprotic solvent is a six-electron reaction [80]. This mechanism is explained in detail in paper II.

2.2.1 Catalysts for 4NP electrocatalysis

The catalysis of 4NP has emerged as a key process in nanoparticle testing. However, the six-electron transfer process still requires suitable catalysts. Several monometallic materials as well as nanoparticle composites have been explored (both chemically and electrochemically) for the conversion of 4NP to 4AP. Monometallic compounds such as Au NPs, Ag NPs, Pt NPs, Pd NPs and other metal electrodes were initially explored and reported in the literature [75,81–84]. Bimetallic nanoparticles for example Ni-Al, Pd-Ag, Au-Cu [85–87], and other materials like boron-doped diamond [88], carbon derivatives such as CNTs [89] and reduced graphene oxide (rGO) [90] are used as electrocatalysts to either detect or reduce 4NP. In addition, electrocatalytic nanocomposites consisting of metals, metal oxides, LDH, chitosan, graphene, and other polymers [91–96] have also been studied for the electro reduction of 4NP. These materials have shown good electron transfer between the electrode and the analyte. In this research, the catalytic performance of materials consisting of Au-TiO_2, Pd-TiO_2, CuFe-LDH and NiFe-LDH were explored using the model compound: 4NP.

3 Catalyst Synthesis

Research is focused on the development of nanoparticle catalysts with distinct properties from the bulk material. The improved properties (particle size, shape, composition, metal-support interaction) play a significant role in the morphology and activity of the nanoparticle catalyst [97]. The top-down and bottom-up approaches are the two most popular methodologies for catalyst synthesis, with the bottom-up being the scientist favourite.

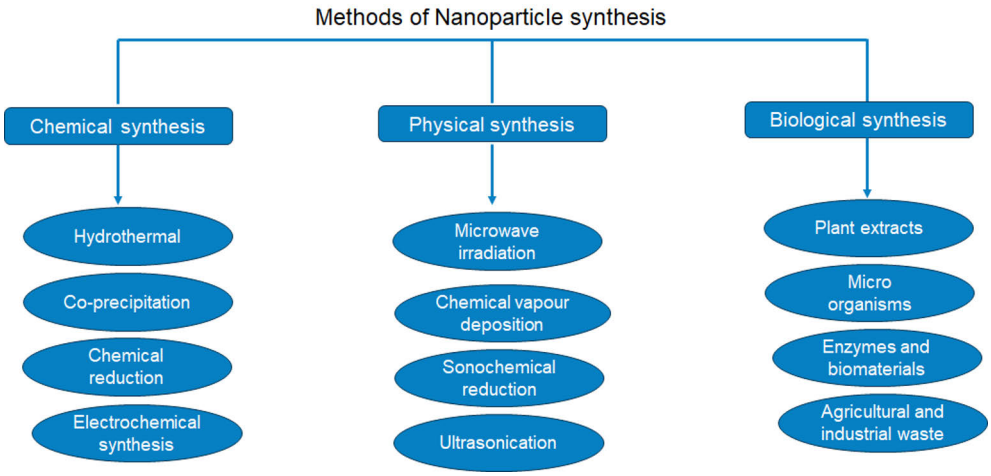

Figure 3. Schematic diagram of methods for nanoparticle synthesis.

Several chemical, physical, and biological methods involving the bottom-up approach have been developed. The chemical synthesis routes mostly studied are the hydrothermal, co-precipitation, chemical reduction and electrochemical methods. Figure 3 shows a cross section of methods reported by literature for the synthesis of nanoparticles. In this research, the hydrothermal synthesis, chemical reduction and co-precipitation method were used for the synthesis of catalyst materials.

3.1 Hydrothermal synthesis

Hydrothermal is coined from the words “Hydro” and “Thermal” meaning water and heat. Hydrothermal synthesis involves reaction in an autoclave at high temperatures (below 300 ºC) and pressure. It is a solution-based reaction, and the reacting substances are usually insoluble at normal temperature and pressure. The pressure can be varied to successfully control the morphology of materials synthesized during the hydrothermal syntheses. The hydrothermal method minimises loss of materials during syntheses and produces catalysts that are stable at high temperature and pressure. The hydrothermal method has, thereafter, given rise to new synthesis methods such as microwave assisted hydrothermal synthesis [98]. The hydrothermal method was used for the synthesis of Cu-TiO_2/rGO. Detailed information on precursor materials and synthesis procedure is presented in paper III.

3.2 Co-precipitation

The co-precipitation method can be used to produce catalytic composites by dissolving and mixing the precursor and support in a single step; in the case of LDH, the metal cations are precipitated in the presence of a base. This is one of the most accessible synthesis techniques that produces catalysts of small particle size and a high metal weight to volume ratio. Because the reaction happens in one-step, supersaturation occurs, and all components nucleate simultaneously. Co-precipitation synthesis is usually followed by washing and ageing steps to remove residual materials that may cause agglomeration during further thermal treatment. Water has been a common solvent used for precipitation methods over the years. With constant research, other solvents such as ethylene glycol, ethanol and mixtures of ethylene glycol and water are now being used as solvents during co-precipitation synthesis [99]. Other synthesis methods similar to the co-precipitation method include polyol synthesis, and microemulsion/inverse microemulsion [100]. In this research, the co-precipitation method was used for the synthesis of LDH (CuFe-LDH and NiFe-LDH) materials (paper II).

3.3 Chemical reduction

In the chemical reduction method, aqueous solutions of the precursor metal salts are chemically reduced using a reducing agent (e.g sodium borohydride, citrate and ascorbate). The reducing agent produces electrons that reduce metal ions to zero valency. During the chemical reduction process, stabilizing agents are also required. These stabilizing agents can also act as reducing agents, resulting in the formation of colloidal nanoparticles. Some of the stabilizing agents used are polyvinyl alcohol, PVA, cetrimethyl ammonium bromide, CTAB and polyvinylpyrrolidone, PVP.

Naturally occurring compounds from plants and microorganisms are also suitable reagents during chemical reduction. The properties of the nanoparticles synthesized through this method can be tuned by varying the concentration of the reducing agent, stabilizer, and metal salt. The chemical reduction method is a preferred method for synthesis due to its simplicity, scalability, and cost effectivity [101]. This was the most used method in this research. Noble metals (Au, Pd) were produced by $NaBH_4$ reduction of metal precursors and further immobilized on support materials (rGO, TiO_2) as presented in paper I and II.

4 Physicochemical Characterization

In this research, physicochemical characterization methods were used to determine the physical and chemical properties of synthesized catalyst materials. A thorough understanding of the structure-reactivity or selectivity relationships, particle size and morphology, elemental composition, and metal-support interaction are essential during the catalytic process. There are several techniques used for catalyst characterization, including FTIR spectroscopy, Raman spectroscopy, mass spectrometry, X-ray diffraction, X-ray photoelectron spectroscopy, electron microscopy, nuclear magnetic resonance, surface area/pore structure, thermogravimetric, and chromatographic techniques. These techniques give information on the nature of the catalyst materials, which are responsible for catalytic activity.

4.1 FTIR spectroscopy

Fourier transform infrared spectroscopy, FTIR is a non-destructive and solvent free technique used to acquire structural information on the organic or inorganic components in a sample. It is a robust technique capable of measuring solid, liquid, and gaseous analytes by *in situ* and remote methods [102]. An FTIR spectrometer consists of an IR source, an interferometer (consisting of the moving and fixed mirror, or a cube corner mirror-set, and a beam splitter) [103] and a detector. In principle, a beam is produced from the IR source, which enters the interferometer to produce an interferogram and consequently enters the sample compartment where the sample absorbs radiation at specific wavelengths, which are unique to the sample. The change in the vibrational energy of the sample is recorded between 400 and 4000 cm^{-1} (mid-IR region) to identify specific functional groups in a sample [104]. The FTIR can be used in the attenuated total reflectance, ATR mode, where minimal sample preparation is required.

In this research, a Bruker Vertex 70 FTIR spectrometer was used for the structural and compositional identification of catalyst materials (Paper I, II, and III). The FTIR was equipped with a Harrick VideoMVPTM diamond ATR accessory and a room temperature deuterated triglycine sulfate, DTGS detector. The spectra were

collected over the range 4000 to 450 cm^{-1} with a spectral resolution of 4 cm^{-1} and a total of 32 scans.

4.2 Raman spectroscopy

Raman spectroscopy is a valuable non-destructive technique used in the identification of compounds. It provides complementary information to FTIR about the vibrational frequency of a sample at the atomic scale. A Raman spectrometer consists of four main components: a monochromatic laser/light source, a monochromator, a sample holder and a detector. The Raman spectroscopic measurement is based on the inelastic scattering of light (the Raman effect) as a function of the monochromatic light source, and the change in the polarizability during vibration is recorded. Various laser types can be used as a Raman excitation source to illuminate the sample. This could be a standalone or integrated laser such as the diode-pumped single-longitudinal laser, single-mode diode lasers and volume Bragg grating lasers. The single-mode diode lasers are the most frequently used in Raman spectroscopy with wavelengths of 785, 830, 980 and 1064 nm. The compact diode-pumped lasers are widely accessible in wavelengths ranging from UV to near-IR (355 - 660 nm). In contrast, the volume Bragg grating lasers are usually combined with diode laser emitters to produce narrow-line emission [105,106]. It is also possible to produce laser light to the sample by other sources such as Raman micro and nano lasers [107], optical fibres [108], and other tuneable lasers (e.g. diamond, silicon) [109,110]. A major advantage of the Raman spectroscopy over other analytical methods is that the Raman measurements require no sample preparation, and the presence of water does not interfere with Raman signals.

In this research, Raman spectroscopy was used to gain information on the structure and properties of graphene-based materials. Information about the D-band (disordered), G-band (graphitic) and I_d/I_g ratio was obtained before and after modification (papers I and III). Raman spectra of graphene-based materials were measured on a Renishaw inVia Qontor Raman microscope equipped with a Leica microscope and a charged coupled device, CCD detector. A 785 nm excitation laser wavelength was employed, and the laser was directed onto each sample through a 20X objective lens, utilizing a grating with a high groove frequency of 1200 grooves/mm.

4.3 X-ray photoelectron spectroscopy

X-ray photoelectron spectroscopy (XPS) is a surface sensitive characterization technique that provides an elemental composition of a sample (with the exception of hydrogen and helium). In principle, an X-ray source containing high-energy photons

irradiates the sample surface and emits electrons (photoelectrons). The binding energy of the core level electron (E_b) can be obtained by measuring the kinetic energy of the photoelectron (E_k) as shown in equation (3)

$$E_b = h_v - E_k - \emptyset \quad (3)$$

where h_v is the X-ray photon energy (XPS photon energy source can be AlKα (1486.6eV) or MgKα (1253.6 eV)) and $\emptyset$ is the work function of the spectrometer (usually 4 - 5 eV) [111]. The XPS provides both qualitative and quantitative information on elements in a sample. The quantitative information is obtained as a relationship between the intensity of the photoelectron peaks and the concentration of the element. While the qualitative information is a function of the chemical shift [112]. In this research, different XPS devices were used. In paper I, the XPS spectra were obtained using a Perkin Elmer PHI 5400 electron spectrometer. The sample was irradiated by a 32-095 X-ray source. The photoelectron spectra were recorded by Mg Kα radiation. In papers II and III, the electronic state of metal components was recorded using a Thermo Scientific Nexsa Surface Analysis System equipped with an Al Kα radiation. Carbon at binding energy of 284.8 eV served as the calibration reference source. The Avantage software was employed to analyse and process the XPS spectra.

4.4 X-ray diffraction

X-ray diffraction (XRD) is a characterization technique based on the interference of monochromatic X-rays and a crystalline material. When Bragg's law (equation (4)) is satisfied, a constructive interference and a diffracted ray is produced [113].

$$n\lambda = 2dsin\theta \quad (4)$$

Braggs law is the relationship between the wavelength of the incident ray (λ), diffraction angle (d) and the lattice spacing (θ) of a given sample. Samples are usually scanned through a range of 2θ angles (5^0 to 70^0) and based on the sample's orientation, lattice diffractions are achieved. Obtained diffraction patterns are matched against the information available in the ICDD (international centre for diffraction data) files to identify the crystallographic phases present in the measured samples.

In paper II the diffraction spectra were measured at room temperature using a Huber G670 detector and copper $K_{\alpha 1}$ radiation (λ=1.5406 Å). The 2θ measurement angle was obtained in the range of 5°-100° with a 30-minute exposure and 10 data scans of the imaging plate. In paper III, the diffraction spectra were analysed using a Malvern Panalytical powder X-ray diffractometer (PXRD), with a CuK_α radiation of 1.5418 Å.

4.5 Transmission and scanning electron microscopy

Transmission electron microscopy, TEM and scanning electron microscopy, SEM provide images of the morphology and topography of a sample. Both SEM and TEM contain an electron gun, a set of objective lenses and an electron aperture. When an electron beam hits the sample, SEM like the name implies, scans the surface of the sample, and uses the emitted (scattered) electrons, while TEM uses the transmitted electrons to provide information on the samples. One major advantage that TEM has over SEM is that TEM can achieve a resolution of 0 to ≈ 0.2 nm, which is higher than the resolution of SEM [114]. SEM provides information of the surface structure and texture of the material while TEM provides information of the internal structure of a material at the atomic scale. In contrast to SEM where thicker samples are required, TEM requires ultrathin samples that can allow electrons to pass through. The depth of field of SEM is higher than in TEM. When SEM is combined with the energy dispersive X-ray spectroscopy, EDX they provide the elemental composition of a material.

In this research, SEM and TEM were used to study the morphology of synthesized materials. The JEM-1400 Plus TEM transmission electron microscope with a 0.38 nm resolution was used to study the size distribution of metal nanoparticles immobilized on the support (papers I, II and III). The microscopic images were captured by OSIS Quemesa 11 Mpix bottom mounted digital camera at an acceleration voltage of 120 kV. Particle size was measured by image J software. In paper II, the morphology and surface characterization of LDH materials was studied using a Thermo-scientific Apreo S FE-SEM at an acceleration voltage of 2.00 KV. Different resolutions were used: 4000X, 12700 X and100000X.

4.6 Thermogravimetric analysis

Thermogravimetric analysis (TGA) is a quantitative thermal technique used to detect the change in mass of a sample with respect to temperature and time. TGA also provides information of the measured samples composition, decomposition, purity, phase transitions, thermal stability, and moisture content. TG curve shows the relationship between the rate of mass change and temperature. In some cases, DSC (differential scanning calorimetry) is coupled with TGA. This is primarily useful for analysing samples that undergo weight changes during measurement. TGA-DSC equipment offers qualitative information that a traditional TGA does not display such as a glass transition, melting, or crystal growth. Additionally, a standard TGA/DSC instrument allows heat flow measurement at extremely high temperatures [115].

The thermal behaviour of Au NPs and Au supported NPs was investigated in this research (paper I) using a TA Instruments SDT Q600 thermo gravimetric analysis-differential scanning calorimetry (TGA-DSC) device. Measurement was performed in N_2 atmosphere at a 100 ml/min flow rate, between 20 °C and 1000 °C.

4.7 Nuclear magnetic resonance spectroscopy

Nuclear magnetic resonance, NMR is an analytical technique used in the identification of molecular structure and impurities present in a sample. Unlike other kinds of spectroscopy that rely on electron excitation, the NMR relies on quantum physics where irradiated energy reacts with nuclei spin when an external magnetic field is applied. The NMR phenomenon is based on the notion that the magnetic properties of an atom's nuclei can be used to obtain information about the chemical composition of a sample. NMR spectrometers consist of a superconducting magnet, a probe, and a control system. The sample is introduced to the magnetic field by placing it into the probe. Radiofrequency pulses are irradiated, the magnetic field aligns the nuclear spins of the atoms in the sample, and then the NMR signals emitted by the sample are collected. NMR signals show the relationship between intensity and chemical shift (ppm). The chemical shift is a function of chemical groups present in the sample. ^{1}H NMR (proton) and ^{13}C NMR (carbon) can be measured [116].

In this research, a Bruker 500 MHz NMR spectrometer with a cryoprobe broadband was used (paper III). A water suppression technique by Bruker was used during measurements.

4.8 High performance liquid chromatography

High performance liquid chromatography, HPLC is a versatile technique used in identification and quantification of samples. HPLC consists of a sample injector, a separation column, an oven (to control column temperature), a solvent delivery system, a detector, and a computer system to display chromatographs. HPLC involves the distribution of the sample between the mobile phase (eluent or analyte) and the stationary phase (column). The choice of mobile phase and stationary phase is an important factor in successful HPLC measurement [117]. In principle, the eluent is pumped into the column through a high-pressure system, then the sample is injected using the automatic sample injector. Separation takes place in the column as a function of the interaction of the sample and the mobile phase. HPLC can be measured in isocratic (same concentration of the mobile phase) or gradient mode (change in mobile phase).

This research used a Hewlett Packard Agilent 1100 series chromatograph equipped with an oven for HPLC measurements (paper III). An ODS HYPERSIL column with a diameter of 250 x 4.6 mm was used. The eluent contained of 1 mM of H_2SO_4 in Millipore water. The column was heated to 60 ^oC while a refractive index detector (RID) was used to identify compounds.

5 Electrochemical Characterization

Electrochemical characterization is a method used to study the properties and behaviour of materials that interact with electric currents or potentials. It allows for the investigation of material performance under applied potential in a variety of corrosion, oxidation, and reduction conditions. Typically, electrochemical characterization requires a cell, potentiostat/bipotentiostat and an electrochemical analyser. Different kinds of cells can be used in electrochemistry but the most popular are the 2- or 3-electrode cell, half-cell, H-cell and flow cell. The electrochemical cell usually consists of a working electrode, WE, reference electrode, RE and counter electrode, CE. The WE is the main electrode under investigation, this can be a metal electrode (Au or Pt) or a GCE. Catalysts can also be deposited on the WE, here the catalyst modified electrode serves as WE. The RE determines the potential of the cell. Hence, the RE is an electrode with a stable potential such as saturated calomel electrode, SCE, silver wire coated with silver chloride, Ag/AgCl, or the reversible hydrogen electrode, RHE. The CE, also known as the auxiliary electrode, completes the electrochemical circuit by allowing the flow of current. Materials often used as CE are Pt wire, graphite, or glassy carbon.

The WE, RE, and CE are connected to the potentiostat with banana plugs or crocodile clamps. The potentiostat controls the potential of the WE in a multielectrode electrochemical cell. The major difference between a potentiostat and a bipotentiostat lies in the bipotentiostats ability to control two WE, as seen in the RRDE set up (Figure 4(a)). The electrochemical analyser is another important device used in electrochemical characterization. It measures the current, voltage, impedance, charge/discharge properties or other electrochemical parameters. Depending on the type of measurement, different electrochemical techniques can be used, such as cyclic voltammetry, linear sweep voltammetry, electrochemical impedance spectroscopy, potentiometry, etc.

In this research, a three-electrode cell was used for all electrochemical characterizations. GCE was chosen as WE, because of its inactivity in many electrochemical reactions. The RE was Ag/AgCl in saturated KCl and the CE was a Pt wire or Pt mesh. Voltammetric and amperometric techniques were used to

evaluate electrochemical performance using either an AutolabPGSTAT101 potentiostat or an Iviumstat A25352 bipotentiostat.

5.1 Cyclic and linear sweep voltammetry

Cyclic voltammetry, CV and linear sweep voltammetry, LSV are potentiodynamic electrochemical techniques used for the initial investigation of catalysts and solvents. In this type of voltammetry, mass transport is by diffusion or migration. Both techniques function by applying a linear potential sweep between the WE and RE at a constant rate (scan rate), while the current flow between the WE and CE is recorded. Thus, a typical CV/LSV voltammogram show the relationship between the current and potential. In principle, the excitation signal of CV linear potential is a triangular waveform [118]. This linear potential can be cycled in the forward and reverse direction resulting in anodic and cathodic peak currents. Thus, CV is the most suitable electrochemical technique to investigate oxidation and reduction reactions (reversible reactions). LSV on the other hand involves a single sweep either in the forward or reverse direction. Thus, LSV is most suitable for irreversible reactions. Aside the triangular linear potential sweep, it is possible to acquire CV/LSV voltammogram using other non-triangular waveforms [119,120] such as square wave voltammetry.

In this research, CV and LSV were used to study the performance of synthesized catalysts in electrochemical reactions. The onset potentials, reduction, and oxidation peak maxima, overpotential and mass transport were determined using these methods.

5.2 Chronoamperometry

Chronoamperometry (CA) is an electrochemical method that studies the rate of change in current with time at a specified potential. It provides information on the stability and activity of electrocatalysts under different potential conditions. In applications such as $ERCO_2$, CA is a method that helps to establish the charging of the electrode double layer and enables product collection and detection. In this research, CA was applied to study the stability of electrocatalysts for $ERCO_2$, and for the collection and detection of products obtained from $ERCO_2$.

5.3 Hydrodynamic voltammetry

Hydrodynamic voltammetry, unlike the other voltammetric techniques discussed earlier, uses two working electrodes in an electrochemical set up: the primary working electrode and the secondary working electrode. It also differs from other

kinds of voltammetry, where mass transport is diffusion or migration controlled. In hydrodynamic voltammetry, the element of controlled forced convection is introduced by rotation. Rotation aids the transport of electroactive species from the bulk to the electrode surface and vice versa. The rate of mass transport can be controlled by adjusting the rotation speed. The electrolyte moves in a smooth, steady, and non-mixable laminar flow towards the electrode. Hence, rotation does not induce a turbulent flow.

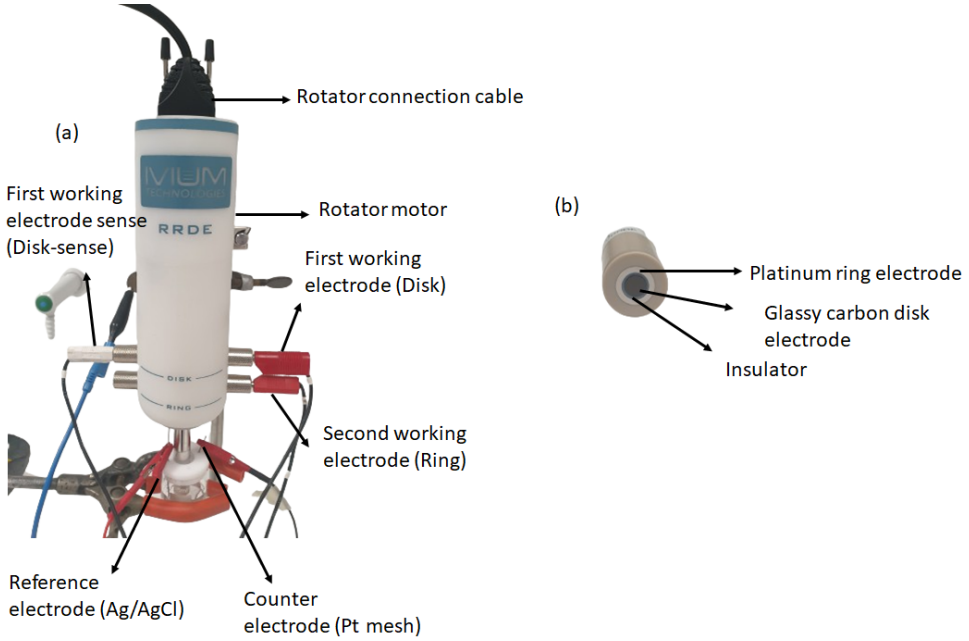

Figure 4. Illustration of (**a**) the RRDE apparatus set up (**b**) RRDE Pt Ring/GC Disc electrode.

There is a variety of hydrodynamic electrodes, but the common ones are the rotating ring disc electrode (RRDE) and the rotating disc electrode (RDE). The RDE is like the traditional working electrode used in voltammetric studies; the major difference is that the RDE can be mounted on a rotator that allows the electrode to spin. The movement of the solution from the bulk to the electrode results in a constant diffusion layer thickness at every rotational speed. The RRDE is similar to the RDE; however, it consists of a disc electrode material of interest (glassy carbon, Pt, Au), and a ring electrode material of interest (Pt, GC, etc.) separated by a non-conducting polytetrafluoroethylene, PTFE insulating sheath (Figure 4). In more advanced electrocatalytic systems, the RRDE can also serve as a RDE, or RRE (rotating ring electrode) by offering the opportunity to turn off or disconnect either the ring (RDE) or the disc (RRE). The RRDE is quite a unique and sensitive

electroanalytical tool that facilitates the transfer of products and intermediates from the disc electrode to the ring electrode. In an ideal electrochemical experiment using an RRDE, electroactive species are generated at the disc electrode and carried by convection resulting from the electrodes rotation to the ring electrode, where it is electrochemically detected. Thus, the disc is the generator while the ring is the collector or detector. When using RRDE in hydrodynamic voltammetry, a bipotentiostat is required to collect the ring and disc currents simultaneously while scanning the potential. The hydrodynamic voltammetric method offers various operational modes that can be used to investigate the kinetics of an electrochemical reaction, especially the study of rapid electrochemical reactions, detection of products and reaction intermediates, understanding and determining reaction mechanisms and determination of faradaic efficiencies. The Faradaic efficiency can be calculated using the RRDE when a single product is formed, e.g. the conversion of CO_2 to CO.

Collection efficiency

Prior to a RRDE experiment, ring calibration and collection efficiency needs to be determined. As discussed earlier, convection aids in sweeping the electroactive species from the disc to the ring for detection. However, not all the electroactive species will get swept to the ring surface. Hence, the collection efficiency is determined, to estimate the effectiveness of the ring in collecting species from the disc. The collection efficiency depends on the geometry of the electrode and the rate of rotation. Therefore, the collection efficiency (N) of an RRDE can be determined experimentally using a well-known redox system such as a ferrocyanide/ferricyanide reaction (potassium hexacyanoferrate reaction) and calculated using the equation (5) below:

$$N = \frac{i_R}{i_D} \tag{5}$$

The empirical collection efficiency is the ratio of the ring limiting current to the disc limiting current at steady-state conditions. In equation (5), i_R and i_D represent the limiting current of the ring and disc respectively. The potassium hexacyanoferrate reaction is a well-known reaction equation (6) below:

$$[Fe(CN)_6]^{3-} + e^- \rightleftharpoons [Fe(CN)_6]^{4-} \tag{6}$$

The electrode is scanned in the negative direction and Fe^{3+} is reduced at the disc and the reduction product (Fe^{2+}) is swept by convection to the ring, where the ring is held at a potential where Fe^{2+} can be oxidized to Fe^{3+}. Thus, the collection efficiency gives information on the amount of Fe^{2+} that migrated to the ring [121]. In this research, the collection efficiency was calculated to be 30 % or 0.30.

Hydrodynamic voltammetry was applied in this research (paper III) using the RRDE. Based on suitable electrochemical configuration, the RRDE also served as the RDE and RRE where necessary. For the RDE experiments, the ring was disconnected and for the RRE experiments, the disc was disconnected. The disc electrode was a glassy carbon electrode, while the ring was a Pt ring electrode. RRDE was employed to detect the products generated during ERCO_2. In principle, CO_2 undergoes reduction at the disc electrode, where products and intermediates are generated, convection as a function of disc rotation, sweeps the generated products to the Pt-ring electrode, where they are detected by oxidation.

6 Summary of Results and Discussion

Paper I investigates the screening of materials for CO_2 electrocatalysis in non-aqueous solution. It examines how the choice of material and electrolyte affects the onset potential for $ERCO_2$ using two types of solvents: organic electrolyte system (0.1 M $TBAPF_6$/ACN) and RTIL ([Emim][NTf_2] and [Hmim][BF_4]). Paper I also focuses on the use of nGO (from cellulose) and its reduced variants (r-nGO, r-nGO-CA) as substrates for immobilizing 1% Au NPs.

Paper II investigates material activity using a model compound: 4NP in organic solvent (0.1 M $TBAPF_6$/ACN). A comparative analysis was conducted between the synthesized LDH materials (CuFe-LDH, NiFe-LDH) and TiO_2 supported metal (Au-TiO_2, Pd-TiO_2) nanoparticles.

Paper III evaluates $ERCO_2$ using the ternary Cu-TiO_2/rGO hybrid material in an aqueous solution (0.5 M $KHCO_3$). The RRDE was employed as a tool to detect the products generated during $ERCO_2$. Non-electrochemical techniques such as NMR and HPLC were employed as a supporting detection tool.

Synthesis parameters such as: synthesis method, stabilizer to reducing agent ratio, the solution pH, support material and metal loading on support were optimized to enable the fabrication of suitable materials for electrocatalytic applications. The effect of these parameters on metal nanoparticle size and activity was taken into consideration. Spectroscopic and microscopic techniques aided in understanding the morphology and characteristics of materials. Electrocatalytic conditions such as electrode material, choice of electrolyte, potential window of electrolyte, method of catalyst deposition on the electrode, amount of catalyst, and rotation speed were also optimized.

6.1 Synthesis of catalysts for CO_2 reduction

Au is one of the most widely studied catalysts for CO_2 reduction due to its ability to form CO [33]. However, Cu is the most promising catalyst for CO_2 reduction due to its initiation of a wide range of products containing oxygenates and hydrocarbons. But selectivity and stability are the major challenges of Cu [122]. Supporting Cu (and other metal NPs) with other conductive supports, such as TiO_2 and rGO materials is

one of the strategies to enhance their catalytic activity and selectivity. Two-dimensional (2D) materials, such as rGO, serve as suitable platforms for growing nanoparticles and improving the rate of charge transfer by creating a synergistic effect between GO and metal nanoparticles [123–125].

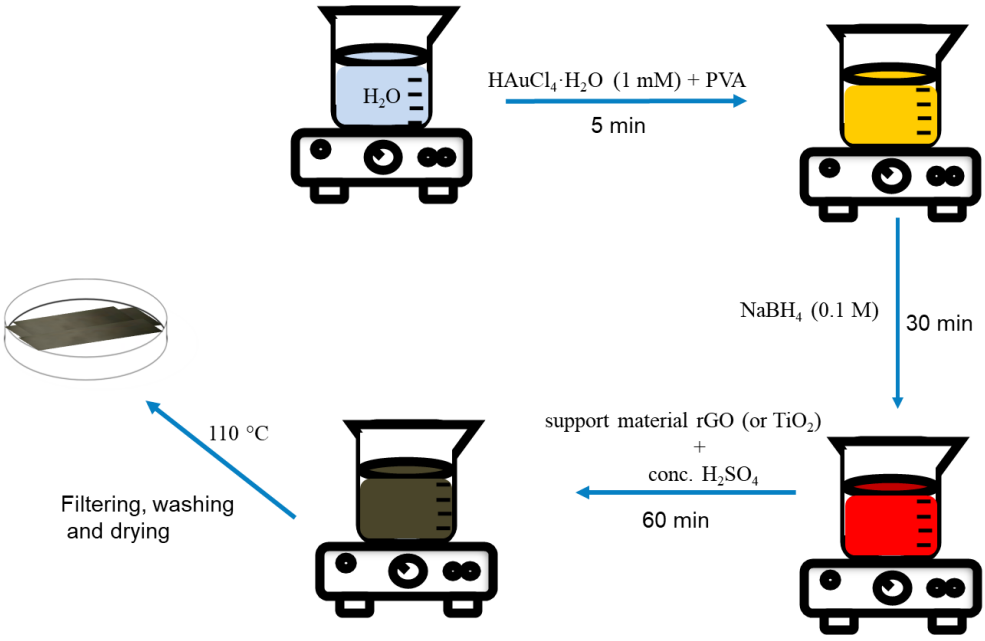

Figure 5. Schematic representation of the synthesis of metal supported nanoparticles.

Literature reports improved stability of alloyed Au and Cu with other metals and metal components [122]. In paper I, graphene oxide (nGO) was prepared from α-cellulose through microwave irradiation. This nGO was then reduced in two ways (i) water reduced, labelled "r-nGO" and (ii) reduced by caffeic acid (CA), labelled "r-nGO-CA" [24,25]. Au was then immobilized on r-nGO and r-nGO-CA at room temperature by a simple one-pot method illustrated in Figure 5 above and described in detail in paper I.

In paper III, a ternary nanocomposite consisting of Cu, TiO_2 and rGO is applied as an electrocatalyst for CO_2 reduction in 0.5 M $KHCO_3$. The TiO_2/rGO support allows for the uniform growth of Cu NPs and the synergistic interaction between Cu, TiO_2 and rGO modifies the electronic properties, rapid transfer of electrons and improves the electrocatalytic activity of Cu for CO_2.

Initially, GO was synthesized by the modified Hummers method [126]. This method is described in detail in paper III. Then TiO_2/rGO (95:5 wt%) was hydrothermally prepared using commercially available TiO_2 and GO from the

modified Hummers method. TiO_2 and GO were ultrasonically treated before being hydrothermally treated in an autoclave for 20 h at 150 °C. The sample was washed with DI water and dried at 25°C for 20 h. The resulting solution was labelled "TiO_2/rGO" because during the hydrothermal synthesis, there was a simultaneous reduction of graphene oxide. Cu was then immobilized on TiO_2/rGO through a slightly similar method as indicated in Figure 5. It is a known fact that Cu is prone to oxidation when in contact with air [127–129]. Therefore, Cu-TiO_2/rGO was synthesized under a nitrogen atmosphere. In practice, in a round bottom flask with nitrogen inlet, an amount of the aqueous metal ion precursor ($Cu(NO_3)_2 \cdot H_2O$) was stabilized by PVA and reduced by 0.1 M $NaBH_4$. A visual observation of the metal ion reduction was evident through a colour change from colourless to brown. Then the colloidal metal ions were immobilized on TiO_2/rGO support. Finally, samples were washed, filtered, and dried in an oven at 110 °C for 20 h.

6.1.1 Composition and properties of CO_2 catalysts

In papers I and III, rGO serves as a support for the growth of metal nanoparticles (Au, Cu) thus providing a synergistic metal-support effect and a reduction in nanoparticle agglomeration. The thermal stability of the as-synthesized materials was evaluated using TGA (paper I), decomposition occurred in three steps. The first mass reduction started at 50 °C, the second step starts at 110 °C and the third step starts at above 500 °C indicating the loss of water and oxygen containing functionalities. At 1000 °C, the residual mass of nGO, r-nGO, and r-nGO-CA, was 14 %, 16 %, and 34 % respectively. The metal supported nanoparticles, on the other hand exhibited a different behaviour with Au/r-nGO retaining a 17 % residual mass, and Au/r-nGO-CA exhibiting a total material loss at 1000 °C due to an increase in oxygen functionalities during synthesis of Au/r-nGO-CA.

Raman spectroscopy is one of the most effective techniques to characterize graphene and graphene-based materials because it gives information about the electronic structure, disorder and defect in crystal structures. Raman spectrum of the as-synthesized graphene-based materials shows a strong D-band at 1300 cm^{-1} and G-band at 1579 cm^{-1} indicating the defective and graphitic nature of the materials (Figure 6 (a)-(d)). In paper I, a blue shift (to a higher wavenumber) was observed for the r-nGO and r-nGO-CA samples. The intensity of the D to G band (I_d/I_g) reduced from 1.06 in nGO to 1.00 in r-nGO and r-nGO-CA. Au/r-nGO and Au/r-nGO-CA did not show any difference in the I_d/I_g ratio when compared to r-nGO and r-nGO-CA. On the other hand, graphene oxide made from the Hummers method (Figure 6(d)) had an I_d/I_g ratio of 0.78. This value increased to 0.9 in TiO_2/rGO and Cu-TiO_2/rGO, as a result of distortion in the GO sheets due to fragmentation during hydrothermal synthesis. Also, the characteristic E_g at 144 cm^{-1} and 640 cm^{-1}, B_{1g} at

396 cm^{-1} and A_{1g} at 516 cm^{-1} of TiO_2 are clearly visible in the TiO_2/rGO and Cu-TiO_2/rGO samples.

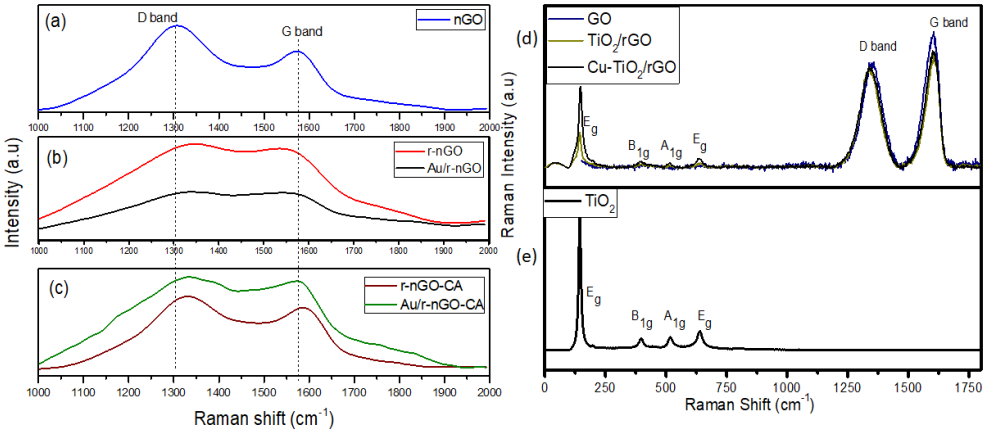

Figure 6. Raman spectra of (**a**) nGO, (**b**) r-nGO, Au/r-nGO (**c**) r-nGO-CA, Au/r-nGO-CA (**d**) GO. TiO_2/rGO, Cu-TiO_2/rGO (**e**) TiO_2. Adopted from Paper I and III.

The morphology and size distribution of synthesized catalyst materials were obtained by TEM (Figure 7). The surface morphology of the graphene-like catalysts (Figure 7(a)-(d)) showed a thin wrinkle like morphology, which is a characteristic of GO and rGO [130]. The metal nanoparticles were uniformly distributed on the rGO sheet of varying sizes and shapes. In paper I, the Au NPs existed predominantly in spheres with particle sizes ranging from 2–5.8 nm (Figure 7(c)-(d)). In paper III, TiO_2 exhibited a spherical and polygonal crystalline shape. However, an actual distinction between the Cu NPs and TiO_2 crystals was not evident (Figure 7(b)) as the Cu NPs were completely submerged in the TiO_2 framework due to oxidation of the Cu NP during synthesis.

The SEM images of Cu-TiO_2/rGO also displayed the distribution of Ti, Cu, O and C, with Cu existing in minute quantity (Figure 7(e)). Furthermore, the presence of the metal Au and Cu and their respective oxidation state was confirmed by XPS (Figure 8). Au in its metallic form Au^0 was confirmed (Figure 8(a)-(b)) and Cu in the combination Cu^0 and Cu^+ was evident (Figure 8(c)). The efforts to prevent the oxidation of Cu proved pointless. However, on the bright side, catalysts with the Cu^0/Cu^+ active site have shown tremendous catalytic activity in electrochemical hydrogenation studies [131–135]. Thus, it was expected that the presence of the Cu^0/Cu^+ active site in Cu-TiO_2/rGO would enhance the catalytic activity of the ternary composite. This was further proved during electrocatalytic measurements (paper III).

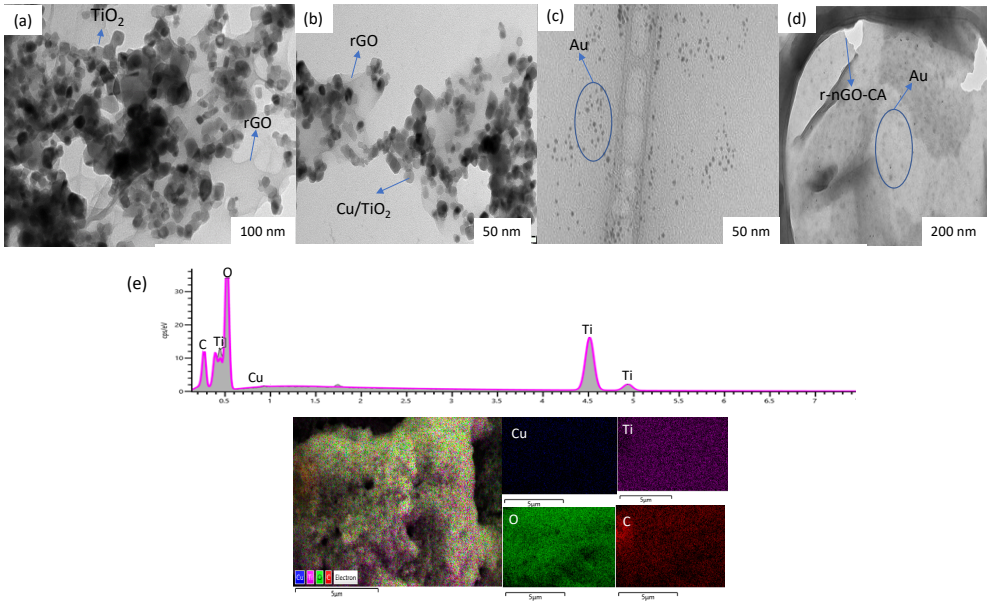

Figure 7. TEM of (**a**) TiO_2/rGO, (**b**) Cu-TiO_2/rGO, (**c**) Au/r-nGO, (**d**) Au/r-nGO-CA, and (**e**) SEM/EDX map of Cu-TiO_2/rGO.

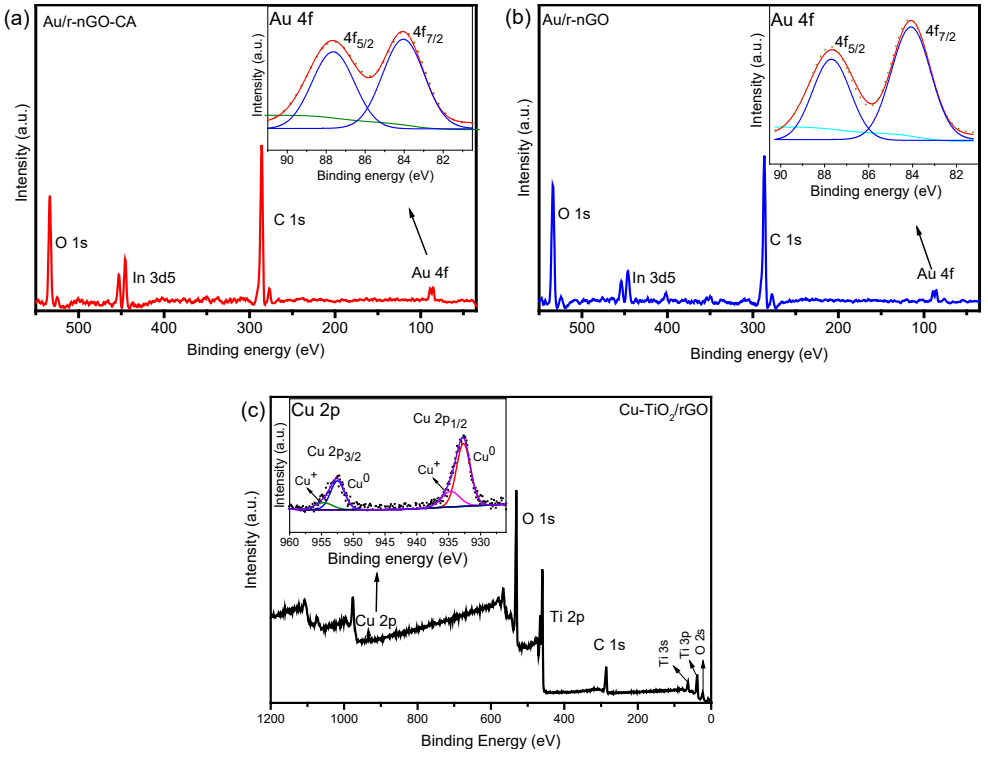

Figure 8. XPS full survey of (**a**) Au/r-nGO-CA (inset: Au 4f core spectra) (**b**) Au/r-nGO (inset: Au 4f core spectra) (**c**) Cu-TiO_2/rGO (inset: Cu 2p core spectra). Adopted from Paper I and III.

6.1.2 CO_2 reduction in non-aqueous solvent

Cellulose derived graphene oxide material (nGO) and its reduced forms (r-nGO, r-nGO-CA) were explored as a suitable support for the growth of Au NPs. To study the effect of the electrolyte and catalyst material on $ERCO_2$, the performance of r-nGO and Au immobilized r-nGO was evaluated for the $ERCO_2$ in organic ($TBAPF_6$/ACN), and RTIL ([Emim][NTf_2] and [Hmim][BF_4]) as seen in paper I. The motivation to choose the imidazolium-based cation is in its ability to form a [Emim]-CO_2 complex and lower the overpotential required to reduce CO_2 [41].

The electrochemical performance of the four catalyst materials (r-nGO, Au/r-nGO, r-nGO-CA and Au/r-nGO-CA) were investigated using CV in N_2 and CO_2 saturated environment. Distinct responses towards CO_2 reduction were observed with all synthesized catalysts. However, Au incorporated rGO samples outperformed the rGO samples in terms of the lower onset potential and increase in current density in both RTIL and $TBAPF_6$/ACN (Figure 9). The improved activity of Au/r-nGO was attributed to the improved reduction of GO to r-nGO which led to a better synergistic effect between Au and rGO. Furthermore, Au/r-nGO showed a lower onset potential for $ERCO_2$ in [Emim][NTf_2] (-1.60 V *vs.* Ag/AgCl) than in [Hmim][BF_4]) (-1.64 *vs.* Ag/AgCl) and $TBAPF_6$/ACN (1.77 V *vs.* Ag/AgCl). This trend is the same with the other catalysts (r-nGO, r-nGO-CA and Au/r-nGO-CA). This can be attributed to the solubility of CO_2 in the electrolytes and the solubility near the electrode surface. Although theoretically, ACN has a higher CO_2 solubility value than [Hmim][BF_4], a higher onset potential was still obtained in [Hmim][BF_4] than $TBAPF_6$/ACN, thus confirming that the stabilization of the catalyst by the imidazolium cation outweighs the solubility effect.

It was interesting to note that anchoring as little as 1 wt% of Au on r-nGO substantially improved the $ERCO_2$ because of its small size, its 0D/2D interface, and the increase in the available active sites which allows for effective adsorption of the reactants while improving the overall activity of the catalyst towards $ERCO_2$. Results obtained showed that the solubility of CO_2 in the solvents and the properties or nature of the electrolyte and the catalysts play a significant role in $ERCO_2$.

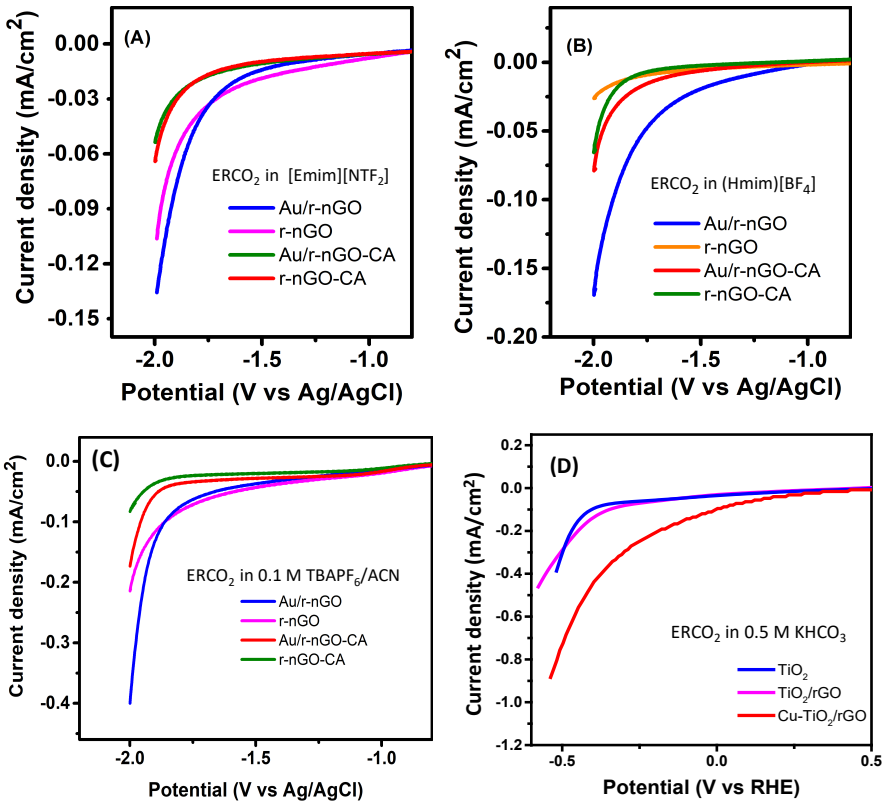

Figure 9. $ERCO_2$ using different catalyst materials in (**a**) [Emim][NTf_2] (**b**) [Hmim][BF_4] (**c**) 0.1 M $TBAPF_6$/ACN at a scan rate of 50 mVs^{-1} and (**d**) 0.5 M $KHCO_3$ at a scan rate of 100 mVs^{-1}. Adopted from Paper I and III.

6.1.3 CO_2 reduction in aqueous solvent

In paper III, the electrochemical performance of three catalysts namely (i) TiO_2, (ii) TiO_2/rGO, (iii) Cu-TiO_2/rGO was evaluated for the reduction of CO_2 in 0.5 M $KHCO_3$ at a rotation of 1600 rpm. The catalysts were evaluated using LSV in N_2 and CO_2 saturated solutions and potentials were recorded *vs.* Ag/AgCl electrode and converted to reversible hydrogen electrode (*vs.* RHE). As expected, Cu-TiO_2/rGO exhibited the lowest onset potential (Figure 9(D)), indicating that the presence of Cu increased the surface-active site in Cu-TiO_2/rGO and enhanced the catalytic activity for $ERCO_2$. The ternary composite showed a positive shift (0.11 V *vs.* RHE) at a current density of -0.49 mA/cm^2. The improved activity of Cu-TiO_2/rGO was also attributed to the presence of Cu^0 and/or Cu^+ phases at the metal/metal oxide interface. With the results obtained from the LSV, and the aim to detect the products formed during $ERCO_2$, the ternary composite Cu-TiO_2/rGO was further investigated for $ERCO_2$ using the RDE and RRDE.

6.1.4 Product analysis

The RRDE was used for its versatility as a sensitive detection tool for the $ERCO_2$. RRDE allows for the reduction on the disc electrode and *in situ* detection on the ring electrode. In paper III, a catalyst decorated GCE disc electrode, and a Pt ring electrode were used for detection studies. To detect or identify products on the RRDE, two approaches were evaluated. (i) The first approach involved a Pt ring calibration of the anticipated products; formic acid, FA and acetic acid, AA. This provided a fundamental understanding of the oxidation potentials of AA and FA within our electrochemical system (detailed information in paper III) (ii) the second approach involved conducting a potential scan on the ring while maintaining a constant potential on the disc. The resulting voltammogram from approach (i) and (ii), were compared.

In approach (i), the Pt ring calibration was recorded in 0.1 M FA and/or 0.1 M AA in CO_2 saturated 0.5 M $KHCO_3$. Results obtained from this approach are detailed in paper III. The Pt ring calibration response of AA was characterized by a large peak from 0.83 to 1.35 V *vs.* RHE, with a peak maximum at 1.2 V *vs.* RHE. The Pt ring response to FA indicated the presence of two anodic peaks. A peak at 0.8 V *vs*. RHE corresponding to FA oxidation. Another anodic peak at 0.5 V *vs.* RHE was also observed.

In approach (ii), constant reductive potentials (-0.1 V, -0.2 V, -0.3 and -0.4 V) were applied on the Cu-TiO_2/rGO GC disc electrode while the Pt ring was cycled from 0 to 1.7 V *vs.* RHE. A large anodic peak stretching from 0.83 to 1.35 V *vs.* RHE was observed at all disc potentials. This peak was centred at 1.2 V, which corresponds to the oxidative peak of AA. No additional peak corresponding to FA was observed. This result is proof of concept that some degree of product selectivity can be obtained by varying the potential applied to the disc. Subsequently, the RRDE was used to calculate faradaic efficiency, FE. For this, the disc was scanned, and the ring was held at the relevant oxidative potential (1.2 V), the disc current and ring current were collected, and the faradaic efficiency was calculated (paper III). It was observed that the FE decreased as the potential became more negative. A FE of 22 %, 15.6 %, 10 % and 7 % were observed for -0.1 V, -0.2 V, -0.3 V and -0.4 V disc potentials respectively.

Additional non-electrochemical techniques (NMR and HPLC) were employed to ascertain product formation. NMR and HPLC analyses were performed on the chronoamperometric samples collected at -0.3 V. AA was detected using NMR and HPLC (Figure 10). This is clear proof that Cu-TiO_2/rGO catalyst in our RRDE system was more selective towards AA formation. This result demonstrates that the RRDE is an effective and sensitive electroanalytical tool suitable for product detection.

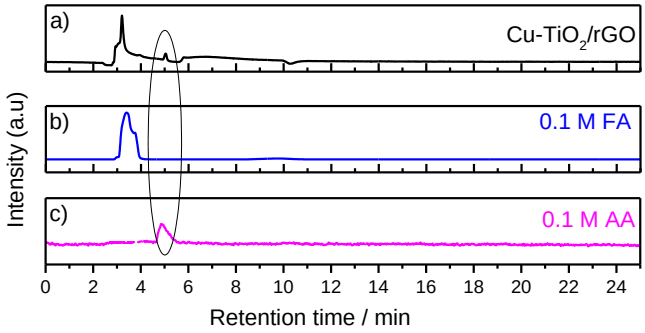

Figure 10. HPLC chromatogram of (**a**) sample collected after chronoamperometric CO_2 reduction at -0.3 V *vs*. RHE using Cu-TiO_2/rGO and 0.1 M of (**b**) formic acid (FA) and (**c**) acetic acid (AA). Adopted from Paper III.

6.2 Synthesis of catalysts for 4NP reduction

Solution-phase synthesis was used to fabricate two distinct sets of catalysts (hydroxide and dioxide) with varying transition metals as active site. The dioxide consists of monometallic Au and Pd supported TiO_2 (Au-TiO_2 and Pd-TiO_2) while the hydroxide consists of layered double hydroxides (NiFe-LDH and CuFe-LDH). Having two sets of catalysts, two different methods of synthesis were applied. The first involved the reduction of the metal ions (Au-TiO_2 and Pd-TiO_2) while the second method involved the co-precipitation method (NiFe-LDH and CuFe-LDH). Since the catalytic activity of NPs are largely dependent on size and shape, NPs with size ranging from 2 - 5 nm were desired.

The dioxide (Au-TiO_2 and Pd-TiO_2) was prepared by a simple, room temperature one-pot method as illustrated in Figure 5 above. The aqueous metal ion precursors were stabilized by PVA and reduced by $NaBH_4$. A visual observation of the metal ion reduction was evident through a colour change from yellow to wine-red (for Au), and yellow to dark brown (for Pd). Then the colloidal metal ions were immobilized on TiO_2 support. In the final step, samples were washed with DI water to remove all unwanted ions formed during synthesis. A visual observation of the clear and colourless filtrate was an indication that all soluble metal ions were removed. TiO_2 is one of the most frequently used support material for immobilization and stabilization of metal NPs due to its cost efficiency and exceptional stability. Also, noble metals possess favourable physical and chemical properties. Thus, incorporating both materials improves their functionality and activity.

The synthesis of the hydroxide materials (NiFe-LDH and CuFe-LDH) took place via a co-precipitation method, where two metal cations (M^{2+}/M^{3+}) are precipitated in the presence of an anion and a base. It is noteworthy that several combinations of LDH is possible by varying the cations, their ratio, and the anions. Theoretically, the

M^{2+}/M^{3+} ratio ranges from 1 to 6. There is no limit to the number of cationic combinations, giving rise to binary and/or ternary LDH materials. In paper II, two cations were used to form the LDH: one divalent and one trivalent. In principle, a mixed metal solution was prepared by dissolving the metal salts (e.g., Ni $(NO_3)_2 \cdot 6H_2O$ and Fe $(NO_3)_3 \cdot 9H_2O$) in the ratio 3:1. NaOH and Na_2CO_3 were added dropwise. The resulting LDH was washed and aged in a digestive bomb to enhance LDH crystallization. LDH samples were then filtered, dried and grinded until a smooth powder was formed. These materials are linked together by hydrogen bonds, and electrostatic interactions between the interlayer anions. Paper II showcases a comparison between the material sets a) Au-TiO_2 *vs.* Pd-TiO_2 b) NiFe-LDH *vs.* CuFe-LDH and c) (a) *vs.* (b).

6.2.1 Morphology of TiO_2 supported catalysts for 4NP electrocatalysis

The composition and surface morphology of all four catalysts studied for 4NP reduction were studied using traditional analytical methods (FTIR, XPS, XRD and TEM) as seen in paper II. The FTIR spectra of Au-TiO_2, Pd-TiO_2, NiFe-LDH and CuFe-LDH (Paper II) revealed a broad band, stretching from 3000 cm^{-1} to 3700 cm^{-1} which is attributed to the O-H stretching mode of absorbed water. The band at ≈1635 cm^{-1} corresponds to the O-H bending vibration of absorbed water. Au-TiO_2, and Pd-TiO_2 exhibited bands at 823 cm^{-1} (tetrahedral Ti-O stretching), 511 cm^{-1} and 611 cm^{-1} which are expected due to the presence of TiO_2 indicating the lattice vibration of Ti-O-Ti network. Additional peaks were also observed on NiFe-LDH and CuFe-LDH, which corresponds to 1356 cm^{-1} (interlayer carbonate), 1373 cm^{-1} (interlayer nitrate), 800 cm^{-1} (metal-oxygen (M-O) vibrations), and 500 cm^{-1} (metal-hydroxyl (M-OH) vibrations).

The XRD pattern of Au-TiO_2 and Pd-TiO_2 was quite difficult to distinguish as the diffraction peaks corresponding to Au and Pd were not observed due to such low concentration (1%) of both metals on the TiO_2 support. Hence the TiO_2 diffraction peaks overshadowed the metal peaks and showed predominantly the anatase and rutile form of TiO_2. On the other hand, NiFe-LDH and CuFe-LDH displayed different XRD patterns though synthesized under identical conditions. The XRD pattern of NiFe-LDH displays the NiFe hydrotalcite layered structure. In contrast, the CuFe-LDH pattern indicates the presence of an LDH altered structure with two strong diffraction peaks at 35.5 ° and 38.7 ° corresponding to Fe_2O_3 and CuO, respectively, achieved as a function of calcination.

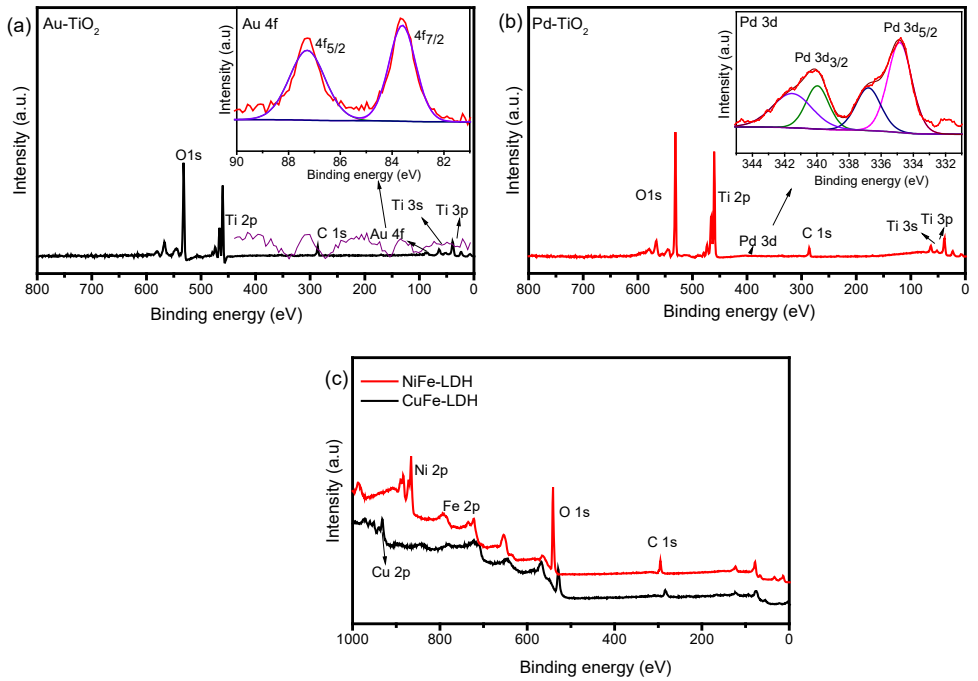

Figure 11. XPS full survey of (**a**) Au-TiO_2 (Inset: Au 4f core level spectra), (**b**) Pd-TiO_2 (Inset: Pd 3d core level spectra), (**c**) NiFe-LDH and CuFe-LDH. Adopted from Paper II.

The presence and electronic state of the metal nanoparticles (Au, Pd) was confirmed by XPS (Figure 11(a)-(b)). Au, Pd, Ti, O and C are clearly identified in the full survey. From the binding energies (87.1 eV and 83.6 eV) in Figure 11(a) (inset), it is evident that Au in Au-TiO_2 exists as Au^0 (in its metallic form) while Pd in Pd-TiO_2 had a Pd^0 core and Pd^{2+} shell (Figure 11(b) (inset)). However, because the XPS is a surface sensitive characterization technique, and doesn't penetrate deep into the core of samples, only the Pd^{2+} shell was observed. The XPS full survey scan indicates the chemical composition of the LDH samples (NiFe-LDH and CuFe-LDH) as represented in Figure 11(c). The presence of Ni, Fe, Cu, C and O was confirmed. The core level element specific spectra were deconvoluted in detail in paper III. The existence of Ni in Ni^{2+} and Ni^{3+}, Cu in Cu^{2+}, and Fe in Fe^{3+} oxidation states were confirmed.

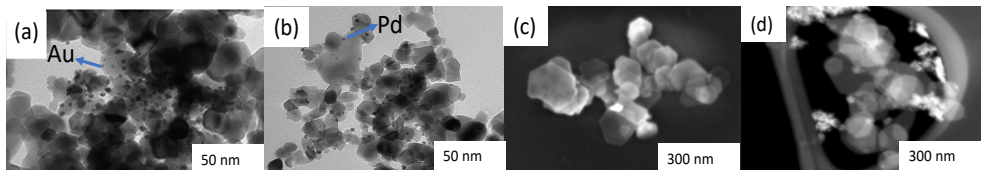

Figure 12. SEM and TEM images of Metal NPs; TEM: (**a**) Au-TiO_2 (**b**) Pd-TiO_2; SEM: (**c**) NiFe-LDH and (**d**) CuFe-LDH. Adopted from paper II.

The morphology of the TiO_2 supported metal nanoparticles (Au, Pd) are quite similar, but reveal a clear difference between the metal nanoparticles (Au, Pd) and the TiO_2 support (Figure 12(a)-(b)). Au NPs (majorly spherical in shape) were distributed uniformly on TiO_2 surface. Au NPs can also be seen in other characteristic shapes (cub-octahedral, decahedral, and icosahedral) with an average particle size distribution of 3 - 5 nm. The spherical and trigonal shaped Pd NPs were sparingly distributed on TiO_2 surface exhibiting an average particle size distribution of 4 - 8 nm. Figure 12(c)-(d) illustrates the SEM images of the hexagonally shaped NiFe-LDH and CuFe-LDH. The CuFe-LDH sample revealed a degree of agglomeration, as the particles are stacked upon one another. This further confirms the result obtained from the XRD, that the LDH structure in the CuFe-LDH sample is altered.

6.2.2 Catalyst performance towards 4NP reduction

Most of the reports published on electrochemical reduction of 4NP have focused on reduction in aqueous solution. However, the electrochemical performance studies of 4NP in aprotic solvent are rare. Hence, paper II set out to examine the performance of two sets of semiconductor materials with transition metal centres for 4NP electro-catalysis in organic solvent.

The electrocatalytic performance of TiO_2 supported Au/Pd and LDH materials was investigated using cyclic voltammetry at room temperature using a three-electrode system in 1 mM 4NP/ 0.1 M $TBAPF_6$/ACN at a scan rate of 50 mV/s. Au-TiO_2, Pd-TiO_2, NiFe-LDH and CuFe-LDH were drop casted on the GCE individually prior to measurement. As a reference, the catalytic contribution of the bare-GCE was recorded, and as expected, bare-GCE showed a weak contribution towards 4NP reduction. However, when catalyst decorated GCE was used, an improvement to the reaction was observed with a distinct jump in peak currents (Paper II).

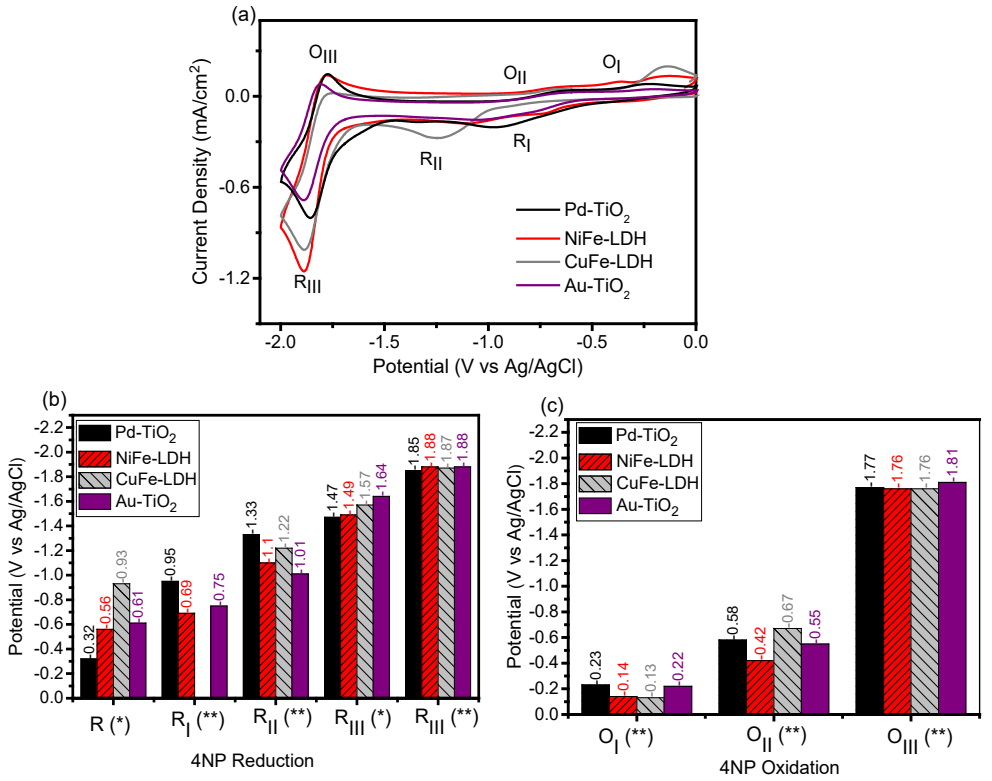

Figure 13. (**a**) CV scan of various catalyst materials measured for 4NP electrocatalysis in 1 mM 4NP/0.1 M $TBAPF_6$/ACN at a scan rate of 50 mVs^{-1} *vs*. Ag/AgCl (Adopted from Paper II). Bar graph comparing onset (*) and peak potential (**) of 4NP (**b**) reduction and (**c**) oxidation.

As evident in (Figure 13(a)), all catalysts were able to reduce 4NP. with reduction peaks R_I - R_{III} and oxidation peaks O_I - O_{III}. According to paper II, the 4NP reduction in organic solvent without a proton source, involves a self-protonation step (R_I) followed by the formation of the radical anion (R_{II}), and the reduction of 4-nitrophenolate anion (R_{III})). Figure 13(b) and (c) show a comparison in the reduction (R_I - R_{III}) and oxidation (O_I - O_{III}) peaks. The order of the onset potential for 4NP reduction on the catalyst studied was -0.32 V, -0.56 V, -0.61 V, -0.93 V for Pd-TiO_2, NiFe-LDH, Au-TiO_2, and CuFe-LDH respectively. Thus, favourable variations in reduction potential and current response were observed across the catalyst series (Pd-TiO_2, Au-TiO_2, CuFe-LDH, and NiFe-LDH), indicating the applicability of these catalysts for 4NP electrocatalysis. Interestingly, among all catalysts studied, Pd-TiO_2 showed the most improved activity with a much lesser onset potential of -0.32 V. In paper II, the improved activity of Pd-TiO_2 was attributed to (i) the Pd^0/Pd^{2+} active site, (ii) the synergistic interaction at the Pd↔TiO_2 interface and (iii) the freely

exposed Pd metal atom available for adsorption. These characteristics allow for the adsorption of 4NP on the Pd-TiO_2 surface thus enhancing the electrocatalytic performance of the catalyst. The catalytic activity followed the order Pd-TiO_2 > NiFe-LDH > Au-TiO_2 > CuFe-LDH. This is due to the difference in the nature of the catalytically active sites. Figure 13(b)-(c) clearly compares the reduction and oxidation peaks with respect to the catalyst material. Furthermore, all catalysts showed improved long-term stability in the reaction with no loss in activity from 1 to 1000 cycles creating an opportunity to expand the use of these electrocatalytic materials for further photoelectrochemical and environmental remediation studies.

7 Conclusions and Future Outlook

Electrocatalysis is the technique of the future, offering an alternative to the use of harsh chemicals and providing a sustainable approach to improving the global economy. Despite its merits, electrocatalysis presents its unique set of challenges. One major challenge involves the search for appropriate electrocatalysts capable of driving various electrochemical reactions. Therefore, this research focused on screening and comparing several nanomaterials (supported and unsupported) for diverse electrocatalytic reactions towards environmental remediation.

In this research, 4NP and CO_2 electrocatalysis was investigated using a range of nanomaterials consisting of metal (Au, Pd, Cu), supported (rGO, TiO_2) and LDH (CuFe, NiFe) materials. The motivation to study these materials was based on their stability, electronic interaction, and their proven activity in other electrochemical applications. Due to scarce information available in the literature for 4NP electrocatalysis in non-aqueous solvent, Pd-TiO_2, Au-TiO_2, CuFe-LDH, and NiFe-LDH were evaluated for 4NP electrocatalysis in ACN. Results demonstrated that the nature of the transition metal active site plays a significant role in the catalyst activity. The activity of LDH materials was slightly lower than Pd-TiO_2 because of better adsorption of the electrolyte on Pd-TiO_2 as a function of its size and metal-support interaction.

Two types of graphene-based support materials were explored as nanoparticle support. One was synthesized using the traditional modified Hummers method (GO), and the other was graphene oxide derived from cellulose (nGO). This research presented nGO (from cellulose) as a new low-cost support material derived through environmentally friendly approaches. Metal nanoparticle immobilized on the microwave-irradiated graphene (r-nGO) and the Hummers graphene, were investigated for $ERCO_2$ in aqueous and non-aqueous solvent. Among all materials studied in both solvent systems, Au/r-nGO was the most suitable for $ERCO_2$ in non-aqueous solvent and Cu-TiO_2/rGO was most suitable in aqueous solvent.

Owing to the improved activity observed for $ERCO_2$ on Cu-TiO_2/rGO and literature knowledge of the well-studied Cu NPs, Cu-TiO_2/rGO was used for further RRDE experiments. The RRDE served as a sensitive tool for the detection of products obtained from $ERCO_2$. The Cu-TiO_2/rGO modified GCE served as the

generator while the Pt ring collected and detected the product. The Pt ring was used to study the electrochemical oxidation peak of the desired products and compared with the product generated during $ERCO_2$. The Cu-TiO_2/rGO facilitated the formation of AA at lower potentials. The Pt ring selectively detected AA at different disc potentials (-0.1 V, -0.2 V, -0.3 V and -0.4 V *vs*. RHE). CO_2 reduction took place at a neutral pH where the hydrogen evolution reaction was suppressed and the reduction of CO_2 to AA was enhanced. Subsequently, NMR and HPLC analysis also confirmed the formation of AA. The quantification of products was out of the scope of this thesis; thus, this thesis simply revealed the RRDE as an efficient tool for the quick screening of materials for $ERCO_2$. In addition, product formation can be selectively tuned, by varying the applied potential during RRDE experiments.

Finally, this research provides valuable insights for the optimization of catalytic processes, highlighting the electrocatalytic techniques as a simple, valuable, and economically feasible tool for tackling environmental remediation. This work provides preliminary efforts to evaluate material suitability in electrocatalytic applications. The insights gained in this research serves as a major foundation required for improving the electrocatalytic performance of metal decorated catalysts. The improvement of these catalysts materials and future study into the RRDE system, would provide alternatives to the use of fossil fuels and other harmful chemicals and positively contribute to environmental remediation.

Acknowledgements

A doctoral journey is an extreme sport that no one can be adequately prepared for. It requires huge determination, stubbornness and mostly a support system. Over the years, I have had immense support; both morally, academically, and financially. For this reason, I want to thank the Department of Chemistry, the Materials Chemistry Research Group, and the doctoral programme in exact sciences (EXACTUS) for the opportunity to conduct my doctoral research. I am particularly grateful for financial support received from them (Department of chemistry and EXACTUS doctoral programme), as well as the Real Estate Foundation, Business Finland, and the Magnus Ehrnrooth Foundation.

I sincerely appreciate Prof. Tanja Kallio, Prof. Pawel Kulesza and Prof. Csaba Janaky for dedicating their time to review my work despite their busy schedules. Profound gratitude goes to my supervisors, Prof. Carita Kvarnström and Adj. Prof. Pia Damlin for their support, friendship, guidance, encouragement, and constructive criticisms throughout this doctoral journey. I am particularly grateful for the faith you both have had in me thus far. Thank you both for always having my back and supporting whatever crazy laboratory ideas I came up with. Special thanks to Mikko Salomäki who was also supervising behind the scenes, thank you for your technical contributions to my entire research.

I also thank Lokesh Kesavan for his support and contributions to scientific discussions and publications. I thank Mauri for cell designs and modifications, thank you Kirsi for ensuring that chemicals were available for experiments. I thank my colleagues Sachin, Milla, Rahul, Ashwini, Lange, Hannah, Sami, Mark, and Cecilia for their friendship and support in and outside the lab.

Thanks to all my friends across the globe (I wish I could mention everyone) for ensuring that I have a life outside research. Special thanks to Dr. Marceline Akieh-Pirkanniemi, Dr. Theresa Bilola, Dr. Elizabeth Eta, Alia Joko, Deborah Afari, and Endurance Boateng for making Turku feel like home for me. To the students I have supervised and co-supervised, it has been an honour to impact knowledge. Though I feel I am the most impacted by all the wonderful experiences and knowledge that you had to share.

Appreciation goes to my family, my dad (Derin Adewumi), for always being ready to research and move mountains where necessary. I will always be your MVP. Thanks to my father who gave me a reason to dream. Thanks to Nkem for being my personal motivational speaker, thanks to my siblings (Oye and Wura) for their encouragement, moral support and love during this research. Thanks to three of my favourite tiny humans (Ini, Elorm and Phoebe) for being a source of joy and laughter in my life. Thanks to OC for your support, love, and patience during this journey, I have indeed been stronger with you.

Finally, I am grateful to the God that has consistently and intentionally been my catalyst, speeding up the reactions of my life. So “Here I raise my Ebenezer, hither by thy help, I have come”.

May 2024
Adefunke O. Koyejo

List of References

[1] A. J. Appleby, Electrocatalysis. In Comprehensive treatise of electrochemistry; B. E. Conway, J. O. Bockris, E. Yeager, S. U. M. Khan, R. E. White (Eds.)*, Springer, Boston*, MA **1983**, *2*, 173–239.

[2] F. Zhang, J. Chen, J. Yang, *Advanced Fiber Materials* **2022**, *4*, 720–735.

[3] A. P. O 'mullane, M. Escudero-Escribano, I. E. L. Stephens, K. Krischer, *ChemPhysChem* **2019**, *20*, 2900–2903.

[4] Z. Xu, X. Wang, *Chemistry – A European Journal* **2020**, *26*, 3897–3897.

[5] S. Anantharaj, K. Karthick, S. Kundu, *Materials Today Energy* **2017**, *6*, 1–26.

[6] Q. Xue, Z. Wang, Y. Ding, F. Li, Y. Chen, *Chinese Journal of Catalysis* **2023**, *45*, 6–16.

[7] S. Hebié, K. B. Kokoh, K. Servat, T. W. Napporn, *Gold Bulletin* **2013**, *46*, 311–318.

[8] H. Wang, H. Hao, Y. Li, *Journal of Physical Chemistry C* **2020**, *124*, 24740–24746.

[9] A. K. Das, C. Retna Raj, *Electrochimica Acta* **2013**, *107*, 592–598.

[10] J. Ni, Q. Cheng, S. Liu, M. Wang, Y. He, T. Qian, C. Yan, J. Lu, *Advanced Functional Materials* **2023**, *33*, 2212483(1) - 2212483(23).

[11] X. Guo, D. J. Guo, X. P. Qiu, L. Q. Chen, W. T. Zhu, *Journal of Power Sources* **2009**, *194*, 281–285.

[12] R. Davis, R. A. Urbanowski, A. K. Gaharwar, *Current Opinion in Biomedical Engineering* **2021**, *20, 1-28*.

[13] M. Chakraborty, M. S. J. Hashmi, *Advances in Materials & Processing Technologies* **2018**, *4*, 573–602.

[14] S. Pei, H. M. Cheng, *Carbon* **2012**, *50*, 3210–3228.

[15] P. Feicht, J. Biskupek, T. E. Gorelik, J. Renner, C. E. Halbig, M. Maranska, F. Puchtler, U. Kaiser, S. Eigler, *Chemistry – A European Journal* **2019**, *25*, 8955–8959.

[16] B. C. Brodie, *Philosophical Transactions of the Royal Society of London* **1859**, *149*, 249–259.

[17] L. Staudenmaier, *Berichte der deutschen chemischen Gesellschaft* **1898**, *31*, 1481–1487.

[18] W. S. Hummers, R. E. Offeman, *Journal of American Chemical Society* **1958**, *80*, 1339.

[19] D. C. Marcano, D. V. Kosynkin, J. M. Berlin, A. Sinitskii, Z. Sun, A. Slesarev, L. B. Alemany, W. Lu, J. M. Tour, *ACS Nano* **2010**, *4*, 4806–4814.

[20] F. Chen, J. Yang, T. Bai, B. Long, X. Zhou, *Journal of Electroanalytical Chemistry* **2016**, *768*, 18–26.

[21] O. Akhavan, K. Bijanzad, A. Mirsepah, *RSC Advances* **2014**, *4*, 20441–20448.

[22] R. Ramli, R. Hidayat, Graphene Oxide Biobased on Biomass Waste: synthesis and Applications, In Graphene – A Wonder Material for Scientists and Engineers; M. Ikram, A. Maqsood, A. Bashir (Eds.), *IntechOpen* **2023,** *12***,** 1-20.

[23] J. K. Saha, A. Dutta, *Waste Biomass Valorization* **2022**, *13*, 1385–1429.

[24] S. Hassanzadeh, N. Aminlashgari, M. Hakkarainen, *ACS Sustainable Chemistry and Engineering* **2015**, *3*, 177–185.

[25] N. B. Erdal, K. H. Adolfsson, T. Pettersson, M. Hakkarainen, *ACS Sustainable Chemistry and Engineering* **2018**, *6*, 1245–1255.

[26] S. Bagheri, N. Muhd Julkapli, S. Bee Abd Hamid, *Scientific World Journal* **2014,** *2014***,** 1-21.

[27] M. Shah, M. K. Al Mesfer, M. Danish, *International Journal of Hydrogen Energy* **2022**, *47*, 8867–8874.
[28] N. Rajalakshmi, N. Lakshmi, K. S. Dhathathreyan, *International Journal of Hydrogen Energy* **2008**, *33*, 7521–7526.
[29] B. Gomathi Thanga Keerthana, T. Solaiyammal, S. Muniyappan, P. Murugakoothan, *Materials Letters* **2018**, *220*, 20–23.
[30] P. Anandgaonker, G. Kulkarni, S. Gaikwad, A. Rajbhoj, *Arabian Journal of Chemistry* **2019**, *12*, 1815–1822.
[31] C. B. D. Marien, C. Marchal, A. Koch, D. Robert, P. Drogui, *Environmental Science and Pollution Research* **2017**, *24*, 12582–12588.
[32] X. Zhang, S. X. Guo, K. A. Gandionco, A. M. Bond, J. Zhang, *Materials Today Advances* **2020**, *7*, 100074(1) -100074(24).
[33] F. Yu, K. Deng, M. Du, W. Wang, F. Liu, D. Liang, *Carbon Capture Science & Technology* **2023**, *6*, 100081(1) -100081(35).
[34] A. S. Kumar, M. Pupo, K. V. Petrov, M. Ramdin, J. R. van Ommen, W. de Jong, R. Kortlever, *Journal of Physical Chemistry C* **2023**, *127*, 12857–12866.
[35] P. J. Welford, B. A. Brookes, J. D. Wadhawan, H. B. McPeak, C. E. W. Hahn, R. G. Compton, *Journal of Physical Chemistry B* **2001**, *105*, 5253–5261.
[36] A. Aljabour, H. Coskun, D. H. Apaydin, F. Ozel, A. W. Hassel, P. Stadler, N. S. Sariciftci, M. Kus, *Applied Catalysis B: Environmental* **2018**, *229*, 163–170.
[37] N. E. Mendieta-Reyes, A. K. Díaz-García, R. Gómez, *ACS Catalysis* **2018**, *8*, 1903–1912.
[38] E. E. L. Tanner, C. Batchelor-McAuley, R. G. Compton, *Journal of Physical Chemistry C* **2016**, *120*, 26442–26447.
[39] S. Sharifi Golru, E. J. Biddinger, *Electrochimica Acta* **2020**, *361*, 136787.
[40] D. Yang, Q. Zhu, B. Han, *The Innovation* **2020**, *1*, 1-25.
[41] B. A. Rosen, A. Salehi-Khojin, M. R. Thorson, W. Zhu, D. T. Whipple, P. J. A. Kenis, R. I. Masel, *Science* **2011**, *334*, 643–644.
[42] A. Hailu, S. K. Shaw, *Energy and Fuels* **2018**, *32*, 12695–12702.
[43] Q. Zhu, J. Ma, X. Kang, X. Sun, H. Liu, J. Hu, Z. Liu, B. Han, *Angewandte Chemie* **2016**, *128*, 9158–9162.
[44] C. Long, X. Li, J. Guo, Y. Shi, S. Liu, Z. Tang, *Small Methods* **2019**, *3, 1-20*.
[45] X. Q. Li, G. Y. Duan, X. X. Yang, L. J. Han, B. H. Xu, *Fundamental Research* **2022**, *2*, 937–945.
[46] H. Ishida, *IntechOpen* **2018,** *2*, 17-40.
[47] Y. Pei, H. Zhong, F. Jin, *Energy Science & Engineering* **2021**, *9*, 1012–1032.
[48] S. Bajracharya, N. Aryal, H. De Wever, D. Pant, Bioelectrochemical Syntheses. In: Aresta, M., Karimi, I., Kawi, S. (eds) An Economy Based on Carbon Dioxide and Water. *Springer, Cham* **2019**, *9*, 327–358.
[49] S. Nitopi, E. Bertheussen, S. B. Scott, X. Liu, A. K. Engstfeld, S. Horch, B. Seger, I. E. L. Stephens, K. Chan, C. Hahn, J. K. Nørskov, T. F. Jaramillo, I. Chorkendorff, *Chemical Reviews* **2019**, *119*, 7610–7672.
[50] Z. Xia, M. Freeman, D. Zhang, B. Yang, L. Lei, Z. Li, Y. Hou, *ChemElectroChem* **2018**, *5*, 253–259.
[51] J. Christophe, T. Doneux, C. Buess-Herman, *Electrocatalysis* **2012**, *3*, 139–146.
[52] A. S. Kumawat, A. Sarkar, *SN Applied Sciences* **2019**, *1*, 1–12.
[53] L. Wan, X. Zhang, J. Cheng, R. Chen, L. Wu, J. Shi, J. Luo, *ACS Catalysis* **2022**, *12*, 2741–2748.
[54] L. Li, X. Jin, X. Yu, M. Zhong, *Frontiers in Chemistry* **2022**, *10*, 1-8.
[55] X. Duan, J. Xu, Z. Wei, J. Ma, S. Guo, S. Wang, H. Liu, S. Dou, *Advanced Materials* **2017**, *29*, 1701784(1)-1701784(20).
[56] B. Kumar, M. Asadi, D. Pisasale, S. Sinha-Ray, B. A. Rosen, R. Haasch, J. Abiade, A. L. Yarin, A. Salehi-Khojin, *Nature Communications* **2013**, *4*, 1-8.

[57] J. Wu, R. M. Yadav, M. Liu, P. P. Sharma, C. S. Tiwary, L. Ma, X. Zou, X. D. Zhou, B. I. Yakobson, J. Lou, P. M. Ajayan, *ACS Nano* **2015**, *9*, 5364–5371.
[58] A. S. Kumawat, A. Sarkar, *Journal of the Electrochemical Society* **2017**, *164*, H1112–H1120.
[59] T. Tsujiguchi, Y. Kawabe, S. Jeong, T. Ohto, S. Kukunuri, H. Kuramochi, Y. Takahashi, T. Nishiuchi, H. Masuda, M. Wakisaka, K. Hu, G. Elumalai, J. I. Fujita, Y. Ito, *ACS Catalysis* **2021**, *11*, 3310–3318.
[60] Q. Li, J. Fu, W. Zhu, Z. Chen, B. Shen, L. Wu, Z. Xi, T. Wang, G. Lu, J. J. Zhu, S. Sun, *Journal of the American Chemical Society* **2017**, *139*, 4290–4293.
[61] H. A. Younus, N. Ahmad, W. Ni, X. Wang, M. Al-Abri, Y. Zhang, F. Verpoort, S. Zhang, *Coordination Chemistry Reviews* **2023**, *493*, 215318.
[62] A. Maurin, M. Robert, *Journal of the American Chemical Society* **2016**, *138*, 2492–2495.
[63] E. A. Mohamed, Z. N. Zahran, Y. Naruta, *Chemistry of Materials* **2017**, *29*, 7140–7150.
[64] M. Wang, K. Torbensen, D. Salvatore, S. Ren, D. Joulié, F. Dumoulin, D. Mendoza, B. Lassalle-Kaiser, U. Işci, C. P. Berlinguette, M. Robert, *Nat Commun* **2019**, *10, 1-8*.
[65] S. Kochrekar, A. Kalekar, S. Mehta, P. Damlin, M. Salomäki, S. Granroth, N. Meltola, K. Joshi, C. Kvarnström, *RSC Advances* **2021**, *11*, 19844–19855.
[66] M. Abdinejad, L. F. B. Wilm, F. Dielmann, H. B. Kraatz, *ACS Sustainable Chemistry & Engineering* **2021**, *9*, 521–530.
[67] T. Amrillah, A. R. Supandi, V. Puspasari, A. Hermawan, Z. W. Seh, *Transactions of Tianjin University* **2022**, *28*, 307–322.
[68] V. Parey, B. M. Abraham, M. V. Jyothirmai, J. K. Singh, *Catalysis Science & Technology* **2022**, *12*, 2223–2231.
[69] K. Kannan, M. H. Sliem, A. M. Abdullah, K. K. Sadasivuni, B. Kumar, *Catalysts* **2020**, *10*, 549(1)-549(15).
[70] N. Li, X. Wang, X. Lu, P. Zhang, W. J. Ong, *Chemistry – A European Journal* **2021**, *27*, 17900–17909.
[71] N. Altaf, S. Liang, R. Iqbal, M. Hayat, T. R. Reina, Q. Wang, *Journal of CO_2 Utilization* **2020**, *40*, 101205(1)-101205(10).
[72] J. He, T. Dou, S. Diao, Y. Wang, X. Zhao, F. Zhang, X. Lei, *ACS Applied Nano Materials* **2023**, *6*, 13543–13550.
[73] J. Huang, Z. Zhang, Y. Wei, L. Guo, J. Liu, C. Zhang, Z. Xue, S. Sun, *Chemistry of Inorganic Materials* **2023**, *1*, 100004(1)- 100004(7).
[74] N. Yamaguchi, R. Nakazato, K. Matsumoto, M. Kakesu, N. C. Rosero-Navarro, A. Miura, K. Tadanaga, *Journal of Asian Ceramic Societies* **2023**, *11*, 406–411.
[75] A. Serrà, R. Artal, M. Pozo, J. Garcia-Amorós, E. Gómez, *Catalysts* **2020**, *10*, 458.
[76] D. Kalaimurugan, P. Sivasankar, K. Durairaj, M. Lakshmanamoorthy, S. Ali Alharbi, S. A. Al Yousef, A. Chinnathambi, S. Venkatesan, *Saudi Journal of Biological Sciences* **2021**, *28*, 833–839.
[77] F. T. Bekena, H. Abdullah, D. H. Kuo, M. A. Zeleke, *Journal of Industrial & Engineering Chemistry* **2019**, *78*, 116–124.
[78] J. Kim, S. Han, Y. Kim, *Korean Journal of Chemical Engineering* **2017**, *34*, 2498–2501.
[79] Q. He, Y. Tian, Y. Wu, J. Liu, G. Li, P. Deng, D. Chen, *Nanomaterials 2019,* **2019**, *9*, 429(1)-429(16).
[80] D. S. Silvester, A. J. Wain, L. Aldous, C. Hardacre, R. G. Compton, *Journal of Electroanalytical Chemistry* **2006**, *596*, 131–140.
[81] Z. Liu, J. Du, C. Qiu, L. Huang, H. Ma, D. Shen, Y. Ding, *Electrochemistry communications* **2009**, *11*, 1365–1368.
[82] P. S. da Silva, B. C. Gasparini, H. A. Magosso, A. Spinelli, *Journal of Hazardous Materials* **2014**, *273*, 70–77.
[83] C. Karuppiah, S. Palanisamy, S. M. Chen, R. Emmanuel, M. A. Ali, P. Muthukrishnan, P. Prakash, F. M. A. Al-Hemaid, *Journal of SolidState Electrochemistry* **2014**, *18*, 1847–1854.

[84] X. Zhang, L. Chen, Y. Zheng, H. Tang, Z. Liu, *Journal of New Materials for Electrochemical Systems* **2019**, *22*, 79–84.
[85] T. Novaković, N. Abazović, T. Savić, M. Čomor, Z. Mojović, *Science of Sintering* **2020**, *52*, 359–370.
[86] A. Shah, M. Akhtar, S. Aftab, A. H. Shah, H. B. Kraatz, *Electrochimica Acta* **2017**, *241*, 281–290.
[87] S. A. Hira, M. Nallal, K. H. Park, *Sensors & Actuators B; Chemical* **2019**, *298*, 126861(1)-126861(12).
[88] Y. Lei, G. Zhao, M. Liu, X. Xiao, Y. Tang, D. Li, *Electroanalysis* **2007**, *19*, 1933–1938.
[89] C. Yang, *Microchimica Acta* **2004**, *148*, 87–92.
[90] P. Wiench, B. Grzyb, Z. González, R. Menéndez, B. Handke, G. Gryglewicz, *Journal of Electroanalytical Chemistry* **2017**, *787*, 80–87.
[91] G. Chang, Y. Luo, W. Lu, X. Qin, A. M. Asiri, A. O. Al-Youbi, X. Sun, *Catalysis Science & Technology* **2012**, *2*, 800–806.
[92] B. Liu, T. Wang, C. Yin, Z. Wei, *Journal of Materials Science* **2014**, *49*, 5398–5405.
[93] S. Dhanavel, T. A. Revathy, A. Padmanaban, V. Narayanan, A. Stephen, *Journal of Materials Science: Materials in Electronics* **2018**, *29*, 14093–14104.
[94] S. B. Khan, K. Akhtar, E. M. Bakhsh, A. M. Asiri, *Appl Surface Science* **2019**, *492*, 726–735.
[95] N. Arora, A. Mehta, A. Mishra, S. Basu, *Applied Clay Science* **2018**, *151*, 1–9.
[96] A. F. Baye, D. H. Han, S. K. Kassahun, R. Appiah-Ntiamoah, H. Kim, *Electrochimica Acta* **2021**, *398*, 139343(1)-139343(13).
[97] L. Liu, A. Corma, *Chemical Reviews* **2018**, *118*, 4981–5079.
[98] Y. X. Gan, A. H. Jayatissa, Z. Yu, X. Chen, M. Li, *Journal of Nanomaterials* **2020,** 2020, 1-3.
[99] P. Munnik, P. E. De Jongh, K. P. De Jong, *Chemical Reviews* **2015**, *115*, 6687–6718.
[100] N. H. Nam, N. H. Luong, *Materials for Biomedical Engineering: Inorganic Micro- and Nanostructures* **2019**, 211–240.
[101] P. Szczyglewska, A. Feliczak-Guzik, I. Nowak, *Molecules **2023**, 28,* 4932(1)- 4932(38).
[102] Z. Bacsik, J. Mink, G. Keresztury, *Applied Spectroscopy Reviews* **2007**, *39*, 295–363.
[103] A. A. Baravkar, R. N. Kale, S. D. Sawant, *International Journal of Pharma & Bio Sciences* **2011,** 2, 513-519.
[104] M. A. Mohamed, J. Jaafar, A. F. Ismail, M. H. D. Othman, M. A. Rahman, *Membrane Characterization* **2017**, 1, 3–29.
[105] R. S. Das, Y. K. Agrawal, *Vibrational Spectroscopy* **2011**, *57*, 163–176.
[106] R. R. Jones, D. C. Hooper, L. Zhang, D. Wolverson, V. K. Valev, *Nanoscale Research Letters* **2019**, *14*, 1–34.
[107] L. Sirleto, *Micromachines (Basel)* **2021**, *12*, 1–5.
[108] J. Li, M. Zhang, *Light: Science & Applications* **2022**, *11*, 1–29.
[109] D. T. Echarri, K. Chrysalidis, V. N. Fedosseev, R. Heinke, B. A. Marsh, B. B. Reich, E. Granados, *Frontiers in Physics* **2022**, *10*, 937976(1)- 937976(11).
[110] S. LaRochelle, M. Ahmadi, W. Shi, *Optica,* **2021**, *8*, 804–810.
[111] C. M. Chan, L. T. Weng, *Materials* **2016**, *9*, 655(1)- 655(29).
[112] A. M. Venezia, *Catalysis Today* **2003**, *77*, 359–370.
[113] R. Soumen, *Pharmaceitica Analytica Acta* **2022**, *13*, 1000688–1000689.
[114] M. Kannan, Transmission Electron Microscope -Principle, Components and Applications. In Fundamentals and applications of nanotechnology. K.S. Subramanian *DAYA Publishing House* **2018,** *9*, 93-100.
[115] A. Fortunato, *Drug-Biomembrane Interaction Studies: The Application of Calorimetric Techniques* **2013**, *5*, 169–212.
[116] B. Diehl, *NMR Spectroscopy in Pharmaceutical Analysis* **2008**, 1, 1–41.
[117] O. E. Petrova, K. Sauer, *Methods in Molecular Biology* **2017**, *1657*, 33-43.
[118] P. T. Kissinger, W. R. Heineman, *J Chem Educ* **1983**, *60*, 702–706.

[119] Y. Uchida, E. Kätelhön, R. G. Compton, *Journal of Electroanalytical Chemistry* **2018**, *818*, 140–148.
[120] Y. Uchida, E. Kätelhön, R. G. Compton, *Journal of Electroanalytical Chemistry* **2017**, *801*, 381–387.
[121] H. M. Fruehwald, O. V. Zenkina, E. B. Easton, *Chemistry Teacher International* **2022**, *4*, 23–37.
[122] M. Ding, Z. Chen, C. Liu, Y. Wang, C. Li, X. Li, T. Zheng, Q. Jiang, C. Xia, *Materials Reports: Energy* **2023**, *3*, 100175(1)- 100175(16).
[123] S. Choi, C. Kim, J. M. Suh, H. W. Jang, *Carbon Energy* **2019**, *1*, 85–108.
[124] D. Ö. Özgür, *Microporous and Mesoporous Materials* **2021**, *314*, 110861(1)- 110861(6).
[125] P. Majumder, R. Gangopadhyay, *RSC Advances* **2022**, *12*, 5686(1)- 5686(34).
[126] P. Damlin, M. Suominen, M. Heinonen, C. Kvarnström, *Carbon* **2015**, *93*, 533–543.
[127] X. Ma, S. Zhou, X. Xu, Q. Du, *Frontiers in Surgery* **2022**, *9,* 1-21.
[128] N. Jardón-Maximino, M. Pérez-Alvarez, R. Sierra-Ávila, C. A. Ávila-Orta, E. Jiménez-Regalado, A. M. Bello, P. González-Morones, G. Cadenas-Pliego, *Journal of Nanomaterials* **2018,** *2018*, 1-9.
[129] M. Nishimoto, R. Tokura, M. T. Nguyen, T. Yonezawa, *Materials Transactions* **2022**, *63*, 663–675.
[130] C. Xiong, C. Zheng, S. Nie, C. Qin, L. Dai, Y. Xu, Y. Ni, *Cellulose* **2021**, *28*, 3733–3743.
[131] C. Si, H. Ban, K. Chen, X. Wang, R. Cao, Q. Yi, Z. Qin, L. Shi, Z. Li, W. Cai, C. Li, *Applied Catalysis A: General* **2020**, *594*, 117466(1)-117466(10).
[132] Q. Wang, Z. Yu, J. Feng, P. Fornasiero, Y. He, D. Li, *ACS Sustainable Chemistry & Engineering* **2020**, *8*, 15288–15298.
[133] L. Sun, J. Han, Q. Ge, X. Zhu, H. Wang, *RSC Advances* **2022**, *12*, 19394–19401.
[134] Z. Xia, Y. Li, J. Wu, Y. C. Huang, W. Zhao, Y. Lu, Y. Pan, X. Yue, Y. Wang, C. L. Dong, S. Wang, Y. Zou, *Science China Chemistry* **2022**, *65*, 2588–2595.
[135] X. Yu, M. Xin, H. Yuan, L. Gao, A. Zheng, E. Xing, X. Zhang, C. Zhang, B. Zong, *Catalysts* **2023**, *13,* 737(1)–737(17).

TURUN
YLIOPISTO
UNIVERSITY
OF TURKU

ISBN 978-951-29-9684-1 (PRINT)
ISBN 978-951-29-9685-8 (PDF)
ISSN 0082-7002 (Print)
ISSN 2343-3175 (Online)

Painosalama Oy, Turku, Finland 2024